Oceanography and Marine Biology: an Annual Review 1996, **34**, 71–107
© A. D. Ansell, R. N. Gibson and Margaret Barnes, Editors
UCL Press

NUTRIENT FLUXES TO PLANKTONIC OSMOTROPHS IN THE PRESENCE OF FLUID MOTION

L. KARP-BOSS, E. BOSS & P. A. JUMARS
University of Washington, School of Oceanography, Box 357940, Seattle, WA 98195–7940, USA

Abstract We present solutions for nutrient transfer to osmotrophs in the full range of flow regimes for which solutions have been published, and we extend some of those solutions to new parameter domains and flow environments. These regimes include stagnant water; steady, uniform flow arising from swimming or sinking; steady shear flows; and fluctuating shear from dissipation of turbulence, as well as the combined effects of turbulence-induced shear and swimming or sinking. Solutions for nutrient fluxes cannot be carried over from one flow regime to another. In all cases, however, mass transfer increases with cell size and with flow velocity. Cell shape becomes particularly important at high flow velocities. For steady, uniform flow arising from sinking or swimming, we find asymptotic analytic and numerical solutions from the engineering literature superior to those in more common use within oceanography. These engineering solutions suggest flow effects an order of magnitude smaller than commonly supposed. A cell radius near 20μm is needed before swimming or sinking can be expected to increase the flux of nutrients, such as nitrate or phosphate, substantially (by ≥50%) over the stagnant-water case. We find sound asymptotic solutions for the case of linear shear and supplement them with numerical solutions of our own to cover the range of cell sizes and shear rates of interest for phytoplankton. We extend them further to cover viscous shears from dissipating turbulence for cells smaller than the Kolmogorov scale (order of 1–6mm in the ocean). Our analysis suggests turbulence effects an order of magnitude greater than previously postulated, with a cell size of 60μm needed to experience substantial gain. Cell rotation, whether induced by the propulsion mechanism in swimming or passively by shear across the cell perimeter, will reduce the rate of nutrient transfer relative to a non-rotating cell unless the axis of rotation parallels the direction of flow. Although in calm water dinoflagellates by swimming are able to increase nutrient uptake, in strong turbulence they may not be able to maintain a rotational axis parallel to the direction of swimming or the direction of shear, resulting in a relative reduction in flux. Conversely, large chains of diatoms and filamentous cyanobacteria that span the radius of the smallest vortices are best able to take advantage of turbulence. Despite these deductions from a diversity of analytic and numerical solutions, unequivocal data to test the contribution of advection to nutrient acquisition by phytoplankton are scarce – owing, in large part, to the inability to visualize, record and thus mimic fluid motions in the vicinities of cells in natural flows.

Introduction

Effects of small-scale fluid motions on diffusional fluxes of nutrients to bacteria and phytoplankton have been reviewed several times (Gavis 1976, Roberts 1981, Lazier & Mann 1989, Mann & Lazier 1991, Kiørboe 1993). It is thus worth asking why it might be worthwhile to visit them yet again. In the process of a review focused much more closely on bacteria, we (Jumars et al. 1993) became aware of several inconsistencies in the published treatments of solute fluxes to osmotrophs. Among the accumulated problems we encountered, one solution (Munk & Riley 1952) is often used for sinking cells while another (Berg & Purcell 1977) is often used for swimming cells, despite the fact that both invoke the identical governing equation and boundary conditions and thus can neither apply to disparate

processes nor both be correct. Unfortunately, we perpetuated several other inconsistencies. In particular, we were not adequately aware of the diversity of field and laboratory flow regimes for which solutions had been given or of the fact that competing solutions had been published for some regimes. The principal purpose of our present review, therefore, is to lay out the diversity of flow regimes plainly and to point out the best of the known solutions for each specific case. We focus on those physical characteristics of the cell and its flow environment that affect nutrient flux.

A secondary purpose is to specify, as accurately as can be done from the existing literature, the size of organism for which relative fluid motion begins to become important in nutrient flux. It has been firmly established that, for diffusion coefficients typical of small molecules in water (of order $10^{-5}cm^2s^{-1}$), 1-μm long, freely-suspended bacteria cannot experience any substantial flux enhancement from the fluid shear about them (Berg & Purcell 1977, Lazier & Mann 1989, Logan & Dettmer 1989). Utilization of slowly diffusing molecules, larger "cell" size or attachment to larger particles, however, can result in significant benefit from relative fluid motion (Roberts 1981, Logan & Hunt 1987, 1988, Lazier & Mann 1989, Logan & Dettmer 1989, Confer & Logan 1991). The ranges of sizes and diffusion coefficients for which such enhancements can become important have been given implicitly or explicitly in several treatments (Logan & Hunt 1987, 1988, Lazier & Mann 1989), but have sometimes been based on equations from inappropriate flow regimes. As with many other real-world biological-physical interactions of interest, these substantial enhancements of fluxes begin in an uncomfortable middle range of parameters for which analytic solutions typically are not available. Our systematic exploration identifies flow regimes and parameter values for which further numerical modelling and laboratory experimentation would be profitable.

The role of fluid motion in the nutrition of planktonic autotrophs and osmotrophs is similar to its role in problems of heat and mass transfer long studied by civil and chemical engineers. Since the governing equations and boundary conditions for the heat-transfer problem and the dilute-solution mass-transfer problem are identical, heat-transfer theory is applicable directly to the study of nutrient fluxes to planktonic osmotrophs. Most of the solutions we present thus come from the engineering literature; we use, however, oceanographic (Appendix I) rather than engineering convention for notation. In keeping with practice in physics and engineering, we use square brackets to denote primary dimensions of length [L], mass [M] and time [T]. To avoid confusion, we avoid the term "convection" and label any organized fluid motion as "advection". In this review diffusion and molecular diffusion are synonymous. Several inconsistencies have occurred because some authors used radii while others used diameters as characteristic dimensions; for consistency, we give characteristic cell sizes as radii. We work from stagnant fluids, through simple, steady shear flows to the three-dimensional, rotational shear flows characteristic of dissipating turbulence. We warn fluid dynamicists that we use the word "particle" exlusively for a solid object of finite dimensions suspended in the flow and not synonymously with a small parcel of water.

We focus on phytoplankton, because it spans the full size range of interest (from a few micrometres to a few millimetres) and comprises a wide diversity of body, chain and colony shapes. Our analysis also applies, however, to metazoan larvae and other free-living planktonic osmotrophs. To save space we refer to the individual as a cell and leave implicit the applicability to multicellular organisms of comparable sizes. We also leave implicit the converse problem of solute leakage from a cell, although it is plain (Jumars et al. 1993, their Fig. 1) that our results apply equally well there. The principal difference is a sign change in the concentration gradient and hence in the flux direction; magnitudes of flow effects on such

fluxes are identical. We also caution that solutions frequently given for a point source or sink cannot adequately describe the problem of solute leakage from or uptake by a cell; an important aspect of fluid motion is the divergence of streamlines around cells.

Mass transfer to cells in stagnant water

Non-motile cells: pure diffusion

Rate of nutrient delivery into a planktonic cell at steady state proceeds at the rate of the slower of two processes in the series, nutrient delivery to the cell membrane and transport across the membrane. If the former is much faster, no nutrient-depleted layer develops around the cell. If the latter is faster, however, nutrient concentration at the cell surface drops below its far-field level, thereby driving a faster delivery rate by diffusion.

The concentration distribution of a nutrient about a planktonic cell in either case is given by the diffusion equation (Crank 1975),

$$\frac{\partial C}{\partial t} = \nabla(D\nabla C)\,, \qquad \text{(Equ. 1)}$$

where D is the diffusion coefficient [$L^2\ T^{-1}$] and C is the concentration of the nutrient of interest. The del operator (∇) indicates partial derivatives in all three spatial dimensions (e.g. in Cartesian co-ordinates $\partial/\partial x+\partial/\partial y+\partial/\partial z$). In a heterogeneous environment like the ocean, D varies in time and space (due to temperature and salinity). Since we are interested in processes at the microscale, D for a given nutrient is assumed to be constant. Thus, $\nabla(D\nabla C) = D\nabla^2 C$.

At steady state ($\partial C/\partial t = 0$) the solution of Equation 1 for a sphere becomes:

$$C = \frac{r_0}{r}(C_0 - C_\infty) + C_\infty\,, \qquad \text{(Equ. 2)}$$

where r_0 is the cell radius, r is the radial distance from the centre of the cell, C_∞ is the far-field concentration and C_0 is concentration at the cell surface. When uptake capacity into the cell exceeds diffusional supply rate, Equation 2 indicates that there exists a nutrient-depleted region in the vicinity of the cell (Koch 1971, Jumars 1993). For convenience, hereafter we refer to this depleted region as the diffusional boundary layer and define it more specifically as the region in which $C \leq 90\%$ of the ambient concentration. By this definition it extends to about nine cell radii away from the cell surface (Fig. 1 herein; Koch 1971, Jumars 1993). The outer limit is arbitrary, since approach to background concentration is asymptotic. The rate at which nutrients will be transported across this diffusional boundary layer can be estimated from the characteristic diffusion timescale (t_D),

$$t_D \equiv \frac{L_c^2}{D}\,, \qquad \text{(Equ. 3)}$$

where L_c is a characteristic length scale (e.g. the thickness of the layer). For a cell with a radius of 10 μm and a diffusional shell 90 μm thick, it will take *c.* 8 s for a molecule such as nitrate or phosphate (D of the order $10^{-5}\,cm^2 s^{-1}$) to cross this layer.

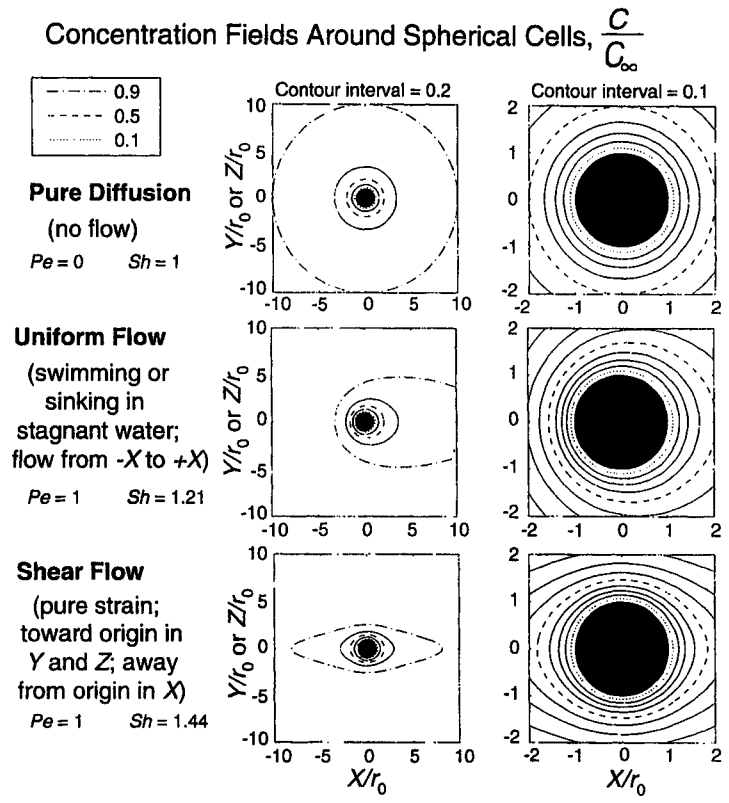

Figure 1 Concentration distributions of a given nutrient around cells (black circles) in three different flow regimes: stagnant water (pure diffusion), uniform flow (i.e. cell swimming or sinking in stagnant water; the cell is moving from right to left so flow is from left to right) and shear flow (uniaxial extensional flow where $\mathbf{E}$ = (2, 0, 0; 0, -1, 0; 0, 0, -1). The third dimension can be visualized by rotation about the x axis. The left panel illustrates the concentration field at distances up to 10 cell radii from the centre of the cell. The right panel is a "blow-up" of the concentration field near the cell surface, up to a distance of 2 radii from the centre of the cell. Concentration values for the case of pure diffusion were obtained by solving Equation 1 at steady state analytically. Values for the two other cases were obtained by solving Equation 11 numerically for $Pe = 1$ to steady state (Appendix II). In the absence of fluid motion a diffusive boundary layer ($C \leq 0.9C_\infty$) extends to about 9 cell radii from the cell surface. Uniform and shear flows distort the boundary layer and steepen the concentration gradient in certain regions. Since transport is dominated by the thinnest regions of the diffusional boundary layer, cells in uniform or shear flow will experience enhanced fluxes compared to non-motile cells in stagnant water.

The diffusional flux of nutrients to a spherical cell (Q_D) depends on the diffusion coefficient, the cell radius (r_0) and the concentration gradient between the cell surface and the ambient water,

$$Q_D = 4\pi D r_0 (C_\infty - C_0), \qquad \text{(Equ. 4)}$$

There are only two means by which the cell can increase the flux to itself without relative fluid motion: increasing r_0 and lowering C_0 (Jumars et al. 1993). There are, however, limits

on the increase achievable. As cell size increases, demand for nutrients increases more rapidly (proportional approximately to r_0^2 cf. Roberts 1981) than does the diffusive flux. In addition, for a given cell size, it is impossible to enhance the flux beyond its value for $C_0 = 0$, when every molecule that reaches the cell surface is absorbed immediately.

Assuming delivery to a spherical cell by molecular diffusion and active uptake of Michaelis–Menten form across the cell membrane, Pasciak & Gavis (1974) introduced a criterion for recognizing transport limitation. They defined the parameter P to be the ratio between diffusional delivery and maximal uptake rates,

$$P \equiv \frac{14.4\pi r_0 D K_m}{V_{max}}, \qquad \text{(Equ. 5)}$$

where V_{max} is the maximal uptake rate [mol cell^{-1} T^{-1}] and K_m is the concentration at which the uptake rate equals $\frac{1}{2}V_{max}$. When P is small, the cell has the capacity to absorb nutrients much faster than the rate at which nutrients can diffuse towards the cell, and transport to the cell membrane becomes limiting. When P is large, the maximal uptake rate is much slower than diffusion, and for such an organism uptake rate will not be controlled by its physical environment. Pasciak & Gavis (1974) applied this criterion to phytoplankton, for which values of K_m and V_{max} were known from laboratory experiments, and thereby established that for some phytoplankton (mostly large cells) transport limitation can be significant. It has also been suggested that under certain conditions uptake of carbon dioxide (Riebesell et al. 1993) and iron (Morel et al. 1991) by phytoplankton and uptake of phosphate by cyanobacteria (Mierle 1985) may become transport limited.

Determining whether uptake plays a role in limitation is clearly important but is outside the scope of our review. For all subsequent analyses, we assume that the cell is a perfect absorber, i.e. that cell-surface nutrient concentration (C_0) equals zero. We do so for two reasons. One is to provide an upper bound on the importance of fluid dynamic effects: if there is no significant effect of fluid motion on uptake for a perfect absorber, then there can be none for an imperfect one. The more obvious reason is for compactness. If kinetics of uptake are known and suspected to be important, they can be included in the problem in the manner shown by Pasciak & Gavis (1974, 1975).

Motile cells: swimming and sinking

Theory

Swimming and sinking are two mechanisms by which a phytoplankter can induce relative fluid motion, steepen its surrounding solute gradients and hence increase the fluxes of nutrients to itself. The nature of the flow in the vicinity of the cell is determined by its body Reynolds number (*Re*). This Reynolds number describes the relative importance of inertial forces compared to viscous forces,

$$Re \equiv \frac{UL_c}{\nu}, \qquad \text{(Equ. 6)}$$

where U is the characteristic velocity, ν is the kinematic viscosity [L^2 T^{-1}] and L_c is the characteristic length scale, in our case the cell radius (r_0). Since typical values of *Re* for plank-

Table 1 Reynolds and Péclet numbers for swimming and sinking phytoplankton.

Organism	Cell radius (μm)	Swimming speed ($\mu m s^{-1}$)	Sinking speed ($\mu m s^{-1}$)	*Re*	*Pe*	Source
Prorocentrum marial-labouriae	6	171	0	1×10^{-3}	1	Kamykowski et al. (1992)
Gyrodinium dorsum	16.5	330	0	5.4×10^{-3}	5.4	Kamykowski et al. (1992)
Dinophysis acuta	33	500	0	1.6×10^{2}	16.5	Sommer (1988)
Coccolithus huxleyi	5 to 6.5	0	3 to 15	1.5×10^{-5} to 9.7×10^{-5}	1.5×10^{-2} to 9.7×10^{2}	Smayda (1970)
Coscinodiscus wailesii	70	0	81 to 347	5.7×10^{-3} to 2.4×10^{-2}	5.7 to 24	Smayda (1970)

tonic micro-organisms are well below unity (Table 1), their environments are dominated by viscous forces, and inertial forces can be neglected.

In the presence of fluid motion the concentration distribution of the nutrient of interest around an organism is given by

$$\frac{\partial C}{\partial t} + \mathbf{U}\nabla C = D\nabla^2 C \qquad \text{(Equ. 7)}$$

where **U** is the three-dimensional velocity field. As a first approximation, we use Stokes' solution for uniform, creeping flow past a stationary, rigid sphere (Leal 1992, Ch. 4) to describe the flow field around cells swimming or sinking in stagnant water. To permit analytic determination of the velocity field and concentration distribution in the neighbourhood of the cell, we assume spherical shape and sufficient spacing between cells to preclude interactions among them.

The boundary conditions applied to Equation 7 are:

$$C = 0 \text{ at } r_0, \text{ and} \qquad \text{(Equ. 8)}$$

$$C = C_\infty \text{ for } r \to \infty. \qquad \text{(Equ. 9)}$$

These boundary conditions set an upper bound for the calculated flux. The flux of a given nutrient (Q) to the cell is determined by the integrated concentration gradient normal to the cell surface:

$$Q = -D\int_A \mathbf{n}\nabla C dA \qquad \text{(Equ. 10)}$$

where A is the cell surface and **n** is an inward unit vector normal to it.

Much of the information and insight about key parameters that determine the concentration distribution in the presence of fluid motion can be obtained via nondimensionalization, without the need to solve the differential equation. Defining $U^* = \mathbf{U}/U$; $C^* = C/C_\infty$ and X^*, Y^*, $Z^* = x/r_0$, y/r_0, z/r_0, the nondimensional form of Equation 7 at steady state becomes

$$Pe\left(\Re^*\nabla^* C^*\right) = \nabla^{*2} C^*, \qquad \text{(Equ. 11)}$$

where each asterisk denotes a nondimensional variable. Corresponding boundary conditions are:

$$C^* = 0 \text{ at } r^* = 1 \qquad \text{(Equ. 12)}$$

$$C^* = 1 \text{ as } r^* \to \infty, \qquad \text{(Equ. 13)}$$

for r^* the nondimensional radial distance from the centre of the cell ($r^* = r/r_0$) and Pe, the dimensionless Péclet number. The Péclet number indicates the effectiveness of advective transport compared with diffusive transport through the fluid over the specified length scale:

$$Pe \equiv \frac{Ur_0}{D}, \qquad \text{(Equ. 14)}$$

where U is the characteristic velocity (swimming and sinking velocities in the case of motile cells). Diffusion dominates transport when $Pe < 1$, and advection dominates when $Pe > 1$. Note that while Reynolds numbers for swimming and sinking planktonic micro-organisms are always smaller than unity, Péclet numbers for large cells can be larger (Table 1). Again, the body Reynolds number of an organism will determine the flow field in its vicinity while the Péclet number will determine the concentration field of nutrients and hence the fluxes.

Since Pe is the only nondimensional parameter arising from the steady-state form of Equation 7, any desired nondimensional quantity determined by the concentration field, namely the nondimensional flux, will be dependent solely on Pe. A measure of this flux is the Sherwood number, Sh (its heat-transfer analogue being the Nusselt number, Nu), which is the ratio between the total flux of nutrients arriving to the cell surface in the presence of fluid motion (Q) and the purely diffusional flux (Q_D):

$$Sh \equiv \frac{Q}{Q_D} = \frac{-D\int_A \mathbf{n}\nabla C dA}{4\pi r_0 D(C_\infty - C_0)}. \qquad \text{(Equ. 15)}$$

Sh thus indicates relative enhancement of flux due to advection. In the case of a spherical cell in stagnant water $Q = Q_D$ and $Sh = Sh_0 = 1$

In the engineering literature the Sherwood number is commonly defined alternatively in terms of the mass-transfer coefficient, k, [L T^{-1}] as $Sh \equiv 2kr_0/D$. In this case, $Sh_0 = 2$. The mass-transfer coefficient is the ratio between the mass flux per unit of area and the concentration gradient between the boundary of interest and the environment (Cussler 1984, Rohsenow & Choi 1961). It can be determined empirically and varies with flow regime and shape of the body. This definition has been adopted in oceanographic applications but in the form $Sh \equiv kr_0/D$ ($Sh_0 = 1$, e.g. Logan & Hunt 1987, 1988). The difference arises from selection of the diameter versus the radius as the characteristic length scale. For the same reason, and hence by the same factor, definition of the Péclet number in the engineering literature often differs from the oceanographic convention, i.e. in the engineering literature it is often $Pe \equiv 2Ur_0/D$. To reduce confusion among oceanographic readers, we have converted all formulas extracted from the engineering literature to the oceanographic convention of Equations 14 and 15 (Appendix I). We make this point and our parameterizations explicit because factors of two based on choice of diameter versus radius as the characteristic dimension have caused some mischief in past comparisons.

In order to examine the effect of fluid motion on nutrient flux a functional relationship between Sh and Pe is sought. First it is necessary to find a solution to Equation 11 that satisfies the boundary conditions 12 and 13. Unfortunately, this problem is too complex to permit exact solution over the full range of Pe. One way to approach it analytically is to derive

asymptotic solutions for limiting values of Péclet numbers. Asymptotic relations between *Sh* and *Pe* have been derived for the two extreme cases, $Pe \ll 1$, when advective effects are relatively minor compared to pure diffusion and $Pe \gg 1$, when the effect of molecular diffusion may be neglected everywhere except for a thin boundary layer at the fluid-cell interface. The major difference between the two is the nature of the dependence of the concentration distribution on flow geometry and hence the nature of the dependence of *Sh* on *Pe*. For low Péclet number, the concentration distribution near the body is governed by molecular diffusion and is therefore relatively insensitive to flow geometry within that region. Cell surface relief smaller than $0.1r_0$ in dimension can have no great effect in this regime. At large distance from the body, however, the form of the velocity field determines the concentration field, so overall body shape and orientation can be influential. At large Péclet number, on the other hand, the effect of molecular diffusion is limited to a very thin layer around the cell, and therefore the concentration distribution will be very sensitive to the flow field in the vicinity of the cell (Leal 1992). Here, small-scale relief on the cell surface can have profound effect. For this reason, flux will be much more sensitive to fine-scale details of cell shape at high *Pe* than at low.

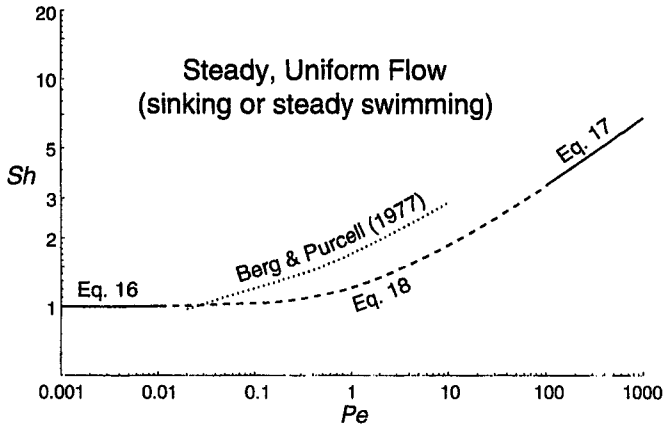

Figure 2 Sherwood number (*Sh*) as a function of Péclet number (*Pe*) for cells moving at a constant velocity in stagnant water or cells fixed in a uniform flow ($Re \ll 1$). Equation 16 was derived by Acrivos & Taylor (1962) for $Pe \ll 1$ and Equation 17 was derived for $Pe \gg 1$ by Acrivos & Goddard (1965). Clift et al. (1978) suggested Equation 18 as a fit to their numerical results; we use it for the region of intermediate *Pe* for which analytic solutions are not available. Berg & Purcell (1977) obtained their relation numerically, but provided no explicit equation. For reasons detailed in the text and in Appendix II, we believe Berg & Purcell's (1977) relation (their Fig. 4) to be inaccurate.

Asymptotic solutions for Equation 11 in the case of steady, uniform, laminar flow and the corresponding boundary conditions (12, 13) yield two relations between *Sh* and *Pe* (Fig. 2). For $Pe \ll 1$ (Acrivos & Taylor 1962)

$$Sh = 1 + \tfrac{1}{2} Pe + \tfrac{1}{2} Pe^2 \ln(Pe) + O\left(Pe^2\right). \qquad \text{(Equ. 16)}$$

For $Pe \gg 1$ (Acrivos & Goddard 1965)

$$Sh = 0.6245Pe^{\frac{1}{3}} + 0.461 + o(1)\,, \qquad \text{(Equ. 17)}$$

where $O(x)$ is read as "of order x", meaning $\geq 0.5x$ but $\leq 5x$, the precise coefficient varying with the details of the situation, and $o(x)$ indicates a term much smaller than the term in brackets. Equations 16 and 17 were derived for the case of heat transfer from a spherical particle and were given in the form of the Nusselt number (*Nu*). For detailed considerations of the use of asymptotic techniques in the analysis of heat-and-mass transfer problems and for lucid derivations of the above solutions we refer the reader to Leal (1992).

Péclet numbers for many if not most phytoplankton fall outside the region for which analytic solutions are available (Table 1). Numerical solutions that include the region of our interest were published by Clift et al. (1978) and Masliyah & Epstein (1972). The former suggested the following relationship for *Sh*, valid for all *Pe* in creeping ($Re < 0.1$), uniform flow:

$$Sh = \tfrac{1}{2}\left(1 + (1 + 2Pe)^{\frac{1}{3}}\right). \qquad \text{(Equ. 18)}$$

So long as very low *Re* is maintained, the above formula agrees within 0.7% in the region $0.001 \leq Pe \leq 0.1$ (Equation 16) and within 2% of the analytic solution (Equation 17) in the region $100 \leq Pe \leq 5000$.

Application of the theory to swimming and sinking cells

Most classes of marine phytoplankton are motile (Sournia 1982). The most thoroughly studied motile phytoplankters are the dinoflagellates; their swimming speeds range from 50 to 500 $\mu m s^{-1}$ (Throndsen 1973, Sournia 1982). A non-motile phytoplankter can sink or rise due to density differences between itself and the surrounding fluid and thus also experience a velocity relative to its environment. For cells of a given size, measured sinking speeds are usually slower than swimming speeds and range from 0 to 347 $\mu m s^{-1}$ (Smayda 1970, his Table VII).

To illustrate the effect of swimming or sinking on the concentration distribution of a given nutrient we solved Equation 11 with the corresponding boundary conditions (12, 13) numerically for $Pe = 1$ (Fig. 1; Appendix II). For both high and low *Pe*, a disproportionate amount of the total flux takes the path of least resistance. As can be seen by inspection of Equation 10, nutrient transport will be dominated by the thinnest regions of the diffusional boundary layer, where diffusion can proceed by far the fastest; characteristic diffusion time varies with the square of this thickness (Equation 3). Hence, total flux arriving to the cell will be larger compared with the purely diffusional flux despite the thickening of the diffusional boundary layer at the "rear" of the cell. Again, some swimming modes may help to "shed" this thickened boundary layer or to thin the thinnest regions even further compared with steady, uniform, Stokes' flow past a sphere. Interestingly enough, it has been reported that chemoreceptors on the cell surface of the motile bacterium *Escherichia coli* are clustered at the pole of the cell rather than being evenly or randomly distributed (Maddock & Shapiro 1993). Such clustering may increase the efficiency of detection, especially if the receptor-rich patch is located at the "leading" pole of the cell (Parkinson & Blair 1993) or where a flagellum locally thins the boundary layer. The advantage is greatly decreased detection time. Berg & Turner (1995) observed that tumbles tend to randomize cell orientation of *E. coli* and that runs of each orientation are of similar duration. They therefore concluded that patches of chemoreceptors at one pole of the

cell do not serve as the bacterium's "nose". Clustering of chemoreceptors or uptake sites at the poles or at other sites of local boundary-layer thinning, however, may still be an effective strategy for other organisms with different modes of swimming.

In order to quantify the enhancement of flux due to swimming and sinking, for the full range of *Pe* values and cell sizes, we use the solutions for mass transfer in steady, uniform flow – namely Equations 16–18. The only differences in our proposed solutions for sinking versus swimming (Fig. 3) arise from differences in the dependence of settling versus swimming speeds on cell size and hence the dependence of *Pe* and *Sh* on cell size. We base swimming speeds on the relationship,

$$U_{\text{swimming}} = \alpha r_0^{\beta}, \qquad \text{(Equ. 19)}$$

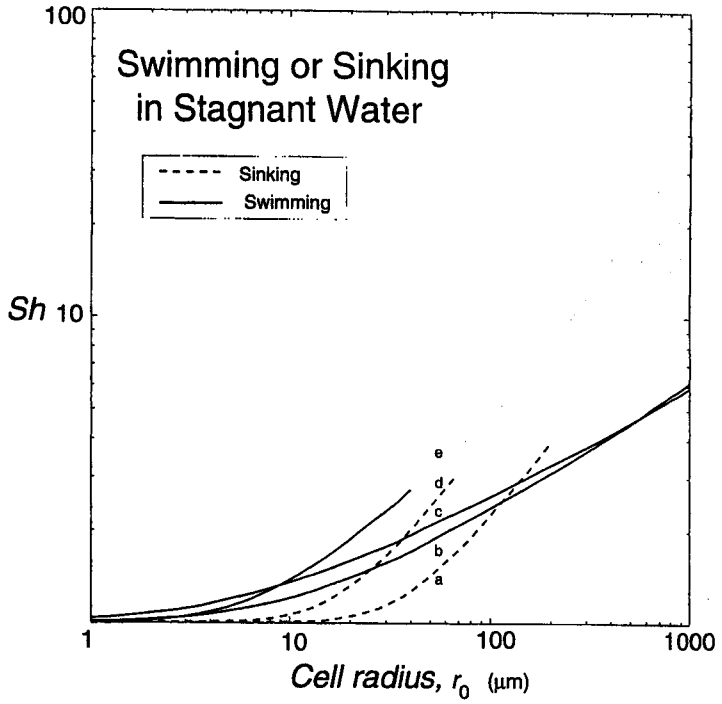

Figure 3 Sherwood number (*Sh*) as a function of cell radius (r_0) for swimming and sinking cells. Both swimming and sinking velocities are functions of cell size; Stokes' equation was used to calculate sinking velocities and the relation $U = \alpha r_0^{\beta}$ was used to calculate swimming velocities. We caution that some correlations between cell size and swimming velocity are very weak; we use them only for illustration. Dashed lines represent sinking cells and solid lines represent swimming cells where: a, sinking cells $\Delta\rho = 0.01$; b, swimming cells $U = 0.16(2r_0)^{0.46}$ (Kamykowski et al. 1992, $R^2 = 0.32$, based on 5 species, ranging in size (r_0) from *c.* 13 to 30 μm); c, swimming cells $U = 93(2r_0)^{0.26}$ (Sommer 1988, $r = 0.38$, based on 19 species, ranging in size (r_0) from *c.* 1 to 40 μm); d, sinking cells $\Delta\rho = 0.1$; and, e, swimming cells $U = 30.66(2r_0)^{1.16}$ (Kamykowski et al. 1992, $R^2 = 0.79$, based on 9 species, ranging in size (r_0) from *c.* 8 to 25 μm). To calculate *Sh* we used equation 16 for $Pe < 0.01$, Equation 18 for $0.01 < Pe < 100$ and Equation 17 for $Pe > 100$. The diffusion coefficient for the calculations of *Pe* was taken to be $1 \times 10^{-5}\,\text{cm}^{-2}\text{s}^{-1}$. The gray segments of curves a, d, and e mark regions for which swimming and sinking velocities extrapolated from the given relations become unrealistic.

which was obtained by Sommer (1988) from the empirical data of Throndsen (1973) and Sournia (1982) and by Kamykowski et al. (1992) from the empirical data of Kamykowski & McCollum (1986). Coefficients α and β vary among species, where $0 < \beta < 2$. We use this function as an example but are aware that for some species its fit is poor. For sinking velocities we used Stokes' equation for sinking spheres (not to be confused with Stokes' solution for the flow field),

$$U_{sinking} = \frac{2gr_0^2(\rho_c - \rho)}{9\mu}, \qquad \text{(Equ. 20)}$$

where g is the gravitational acceleration constant ($980 cm s^{-2}$), ρ_c and ρ are the densities of the cell and fluid, respectively [ML^{-3}], and μ is dynamic viscosity (approximately $0.01 g cm^{-1} s^{-1}$; for more accurate values as a function of temperature and salinity see Jumars et al. 1993). Excess densities ($\rho_c - \rho$) used for the calculations were 0.1 and $0.01 g cm^{-3}$ (Van Ierland & Peperzak 1984). The diffusion coefficient (D) for nutrients such as nitrate and phosphate is $O(10^{-5}) cm^2 s^{-1}$. For calculations of Péclet number, D was taken to be $1 \times 10^{-5} cm^2 s^{-1}$.

For both swimming and sinking, nondimensional mass transfer to the cell depends directly (but not necessarily linearly) on cell size and cell velocity relative to the water and inversely on the diffusion coefficient, as implied from the relationship between *Sh* and *Pe*. Realistic swimming or sinking speeds do not increase substantially the flux of nutrients such as nitrate or phosphate to small cells (Fig. 3). Critical cell sizes for which swimming and sinking begin to become important (to be conservative, we consider a substantial enhancement as an increase of 50% or more of the flux) will vary with the parameters determining the specific dependence (Table 2).

Table 2 Predicted cell radii for 50 and 100% increase in flux, based on equations 16–18.

	Predicted cell radius (mm)	
Mode of motility	50% increase in flux	100% increase in flux
Swimming, $U = 30.66(2r_0)^{1.16}$	12	22
Swimming, $U = 93(2r_0)^{0.26}$	15	44
Swimming, $U = 0.16(2r_0)^{0.46}$	25	61
Sinking, $\Delta\rho = 0.1$	25	39
Sinking $\Delta\rho = 0.01$	54	84
Turbulence-induced shear ($\varepsilon = 10^{-2} cm^2 sec^{-3}$)	63–100 (calculated from the lower and upper limits for interpolation; (see Fig. 6)	167–202 (calculated from the lower and upper limits for interpolation; (see Fig. 6)

Motility, however, may become beneficial for small cells if larger molecules are considered. Amon & Benner (1994) have shown that high-molecular-weight, dissolved, organic matter (HMW DOM; molecules smaller than $0.1 \mu m$ but larger than $0.001 \mu m$) is more readily remineralized by bacteria than low-molecular weight DOM (molecules smaller than $0.001 \mu m$). Diffusion coefficients (at 20°C) for HMW DOM can range from *c.* $10^{-6} cm^2 s^{-1}$ to *c.* $10^{-8} cm^2 s^{-1}$ (estimated from the size cut-off for HMW DOM following Cussler 1984). For a bacterium $0.45 \mu m$ in radius, swimming at $20 \mu m s^{-1}$ will not appreciably enhance the flux of molecules having a diffusion coefficient $O(10^{-5}) cm^2 s^{-1}$ but will increase the flux of

molecules with a diffusion coefficient $O(10^{-8})cm^2s^{-1}$ by 80%. The predicted contribution of advective flux also depends on ambient temperature through the latter's effect on the diffusion coefficient of the solute (Cussler 1984) and on viscosity (Korson et al. 1969) and thus on sinking velocities and velocity gradients in the vicinity of the cell. While mixotrophy and particle feeding are outside the scope of our review, we note that the diffusion coefficients used to characterize Brownian motion of particles are far smaller than diffusion coefficients for molecules, so that fluid motion may have substantial effect (Shimeta 1993, Shimeta et al. 1995).

The theory we have applied (i.e. Equations 16–18) is at odds with previous, widely cited theory that examined the utility of swimming and sinking in enhancing nutrient fluxes. Munk & Riley (1952), who examined effects of sinking on nutrient absorption by phytoplankton cells of varying shapes, applied an analytic solution derived by Kronig & Bruijsten (1951) for spheres in uniform flow at $Pe \ll 1$:

$$Sh = 1 + \tfrac{1}{2} Pe + 0.6 Pe^2 . \qquad \text{(Equ. 21)}$$

Other solutions were not available to them at the time. For the first-order approximation, the correlation they used agrees with Equation 16. For larger values of *Pe*, Munk & Riley (1952) used the empirical relationship given by Kramer (1946), which is valid only for $Re > 1$ and therefore not for sinking phytoplankton. No explicit relation between *Sh* and *Pe* was given by Munk & Riley (1952) for the region of intermediate Péclet numbers. Their estimates for that region were obtained by interpolation between the analytical and empirical relationships.

Berg & Purcell (1977), who examined the effect of swimming on nutrient uptake, solved Equation 11 with boundary conditions 12 and 13 numerically. They did not provide an equation for the relation between relative increase in mass transfer and Péclet number, but their model results suggested that for $Pe \ll 1$ the increase in nutrient flux is proportional to Pe^2, while for the case of $Pe > 1$ (though they did not examine the increase of flux beyond $Pe = 10$) the flux is proportional to $Pe^{1/3}$. Berg & Purcell (1977) argued that the increase of flux in the neighbourhood of $U = 0$ must depend on an even power of U since it cannot depend on the direction of the motion and cannot have a singularity at $U = 0$. The total nondimensional flux, integrated over the whole surface area of a spherical cell, however, does not depend on the direction of the flow – only on the magnitude of the velocity (as implied from the relation $Sh = f(Pe)$), and therefore we find no particular reason to argue for dependence of an even power. Moreover, the shape of the curve implied by Berg & Purcell's correlations (the exponent of *Pe* going from 2 to 1/3, i.e. a sigmoidal curve) implies an intermediate Péclet number for which the fractional increase of flux ($\partial Sh/\partial Pe$) is maximal. Since we are dealing exclusively with small *Re*, changes in the flux as a function of *Pe* are expected to be gradual and monotonic. We cannot find any physical basis for steeper change at any particular velocity, cell size or diffusion coefficient. We speculate on the source of the discrepancy between Berg & Purcell's (1977) numerical solution and the analytical solution or our numerical solution in Appendix II.

Berg & Purcell's estimate for the increase in the nondimensional flux due to advection is higher than predicted by Equation 18 in the region $Pe > 0.04$ (Fig. 2). For example, Berg & Purcell estimated *c.* 76% increase in the flux for $Pe = 1$ while Equation 18 and the results of our numerical model (Fig. 1; Appendix II) predict an increase of 22 and 21%, respectively. In order to double the flux of nutrients to the cell, the Péclet number should be of the order 2.5 according to Berg & Purcell (1977) and 13 according to Equation 18 (Fig. 2). Estimates of the effect of swimming on nutrient transfer (Roberts 1981, Goldman 1984, Sommer 1988, Lazier & Mann 1989, Mann & Lazier 1992) that were calculated from the graphical presen-

tation of Berg & Purcell (1977) must, therefore, over-estimate the contribution of motility to nutrient fluxes. Rather than endangering Berg & Purcell's central conclusion that swimming will be ineffective in enhancing the flux of rapidly diffusing ($D = 10^{-5}\text{cm}^2\text{s}^{-1}$) nutrients to bacteria, the analytic solution makes it even more unassailable.

Our results (Fig. 3) indicate that there is no one mechanism that is always more beneficial in enhancing the flux, and call into question Gavis's (1976) conclusion that swimming is more effective than sinking in reducing diffusional transport limitation. Other factors, such as the cost of swimming and the risk of being transported away from the euphotic zone when sinking rapidly, should be taken into account, however, when the benefits of each mode are considered. Dependence of swimming speed on cell size varies with mode of self propulsion, i.e. planar wave motion, helical wave motion or a combination of both. For instance, cells driven by a flagellum beating with a helical wave rotate as they swim (Chwang & Wu 1971, Brennen & Winet 1977). Smaller cells tend to have higher rotational velocities that slow their translational velocities compared to larger cells. As cell size increases, however, drag increases, too, and larger cells that may escape the problem of rotation face increasing drag, which tends to reduce their translational velocities. Thus, for a phytoplankter using this mode of swimming there is an intermediate size for which swimming speed is maximal (Brennen & Winet 1977, Kamykowski & McCollum 1986). Sinking speeds may also deviate from the predicted relation with cell size. Empirical data on sinking speeds as a function of cell size indicate that the slope can be smaller than the value of 2 predicted by Stokes' law, no doubt the result of a correlation between size and excess density (Waite et al. 1992). Sinking or rising speeds may vary with nutrient and light conditions (Culver & Smith 1989) and depend on the growth phase of the cell (Eppley et al. 1967, Smayda 1970). Among the majority of planktonic diatoms, nutrient-depleted cells sink more rapidly than nutrient-replete cells (Titman & Kilham 1976, Smetacek 1985, Waite et al. 1992). Within a species there may be variations in sinking speeds of a factor of two or more with varying nutritional status of the cell, accompanied by relatively small changes in cell size (Jackson & Lochmann 1993). We have applied those correlations, nevertheless, to demonstrate that effects of sinking and especially swimming on the flux of nutrients cannot be generalized and that the dependence of *Sh* on cell size will vary with the mode of motion (Table 3).

Effects of self-induced rotation vary with orientation of the rotational axis and with *Pe*. Rotation, if strong, can reduce advective contribution to flux when it causes streamlines to curve and sometimes even to close. Water can circulate around the cell longer before being replaced by new water. Advective flux to a rotating, swimming cell will decrease relative to a non-rotating swimmer, however, only if the cell has a component of translation in a direction perpendicular to the axis of rotation, and the decrease will be most important at high *Pe* when advection dominates transport. At low *Pe* diffusion is the dominant transport mechanism, and rotation will distort the diffusive boundary layer around the cell by shearing water parcels in its vicinity (as a result of the no-slip boundary condition at the cell surface).

Table 3 Dependence of *Sh* on cell radius for swimming and sinking cells and for neutrally buoyant cells suspended in turbulent water.

Flow generated by	$Pe \ll 1$	$Pe \gg 1$
Swimming	$Sh \propto r_0^{1+\beta}$ where $0<\beta<2$	$Sh \propto r_0^{(1+\beta)/3}$ where $0<\beta<2$
Sinking	$Sh \propto r_0^3$	$Sh \propto r_0$
Turbulence/shear	$Sh \propto r_0$	$Sh \propto r_0^{2/3}$

This distortion of the diffusive layer can increase diffusional flux relative to a swimming, non-rotating cell. The effect, however, will probably be very small. The axis of rotation of dinoflagellates propagating in a helical wave is parallel to the direction of motion. By our arguments such a swimming mode will still provide a flux advantage across the full *Pe* range, and it appears to carry little cost for most ciliary and flagellar mechanisms (Purcell 1977, Raven 1982, Raven & Richardson 1984, Fenchel 1987) unless very high speeds (in terms of body lengths per unit of time) are achieved (Mitchell 1991).

Our and prior applications of the same flow field (Stokes' flow) to both swimming and sinking are, at best, rough approximations. Swimming and sinking cells differ in the near-cell details of flow streamlines around them. While streamlines around sinking cells closely resemble Stokes' flow, in the near field, streamlines around swimming cells may differ (Keller & Wu 1977) and will vary among species, depending on the mode of swimming. Precise determinations of flow fields around swimming cells require numerical models and observations specific to each case. Our application of Stokes' flow is clearly most questionable for swimming at high *Pe*. Motions near swimming appendages will be unsteady, thinning the diffusional boundary locally. Because the diffusion time scale varies with the square of diffusion distance, such thinning is disproportionately important relative to unsteady thickening in other regions. Hence at high *Pe* we will underestimate the true *Sh* and advective contribution to the flux. Since the details depend on local thinning, there can be no general solution; specific solutions will be time dependent and will also be highly dependent on the mode of swimming and the shape of the cell. In short, flux to swimming cells appears to be a fertile ground for detailed numerical simulation.

Effect of shape on the nutrient flux

Among phytoplankton, relatively few species are spherical. Morphological diversity in nature suggests that each form has a slight advantage in a particular set of conditions (Munk & Reilly 1956, Sournia 1982). Grazing, drag and nutrient absorption are the commonly suggested selective factors leading to the observed diversity (Sournia 1982). The non-dimensional flux to a body of an arbitrary shape (i.e. its *Sh*) is defined as the total flux arriving to the cell surface in the presence of fluid motion normalized to the purely diffusional flux arriving to a sphere with an equivalent surface area (Leal 1992). A general solution for mass transfer to a body of arbitrary shape in steady flow for $Pe \ll 1$ was given by Brenner (1963):

$$\frac{Sh}{Sh_0} = 1 + \tfrac{1}{2} Sh_0 Pe + \tfrac{1}{2} Sh_0 f Pe^2 \ln Pe + O(Pe^2), \qquad \text{(Equ. 22)}$$

where f is the dimensionless drag on the body [f = (drag force)/$6\pi\mu r_0 U_\infty$, with $f = 1$ for a sphere] and Sh_0 is the mass transfer to the shape of interest in the case of pure diffusion and depends upon the geometry of the body. Sh_0 can be estimated for each shape from theory (Clift et al. 1978, their table 4.2) or by experiment.

Dimensionless drag, f, depends on orientation of the body relative to its direction of motion. From experience at high *Re*, one might assume that a sinking cell would orient itself such that the drag is maximized (for example, that a cylindrical cell would sink with its largest projected area perpendicular to the falling axis). For $Re < 0.1$, however, the initial (arbitrary) orientation will be kept during sinking (McNown & Malaika 1950) unless weight is unevenly distributed in the cell (Hutchinson 1967, Sournia 1982). Values and expressions

for the resistance of spheroids in uniform flow were given by Happel & Brenner (1965, their table 4–26.1) and Clift et al. (1978, their table 4.1).

For $Pe >> 1$ the relationship $Sh = cPe^{1/3}$ holds for rigid bodies of arbitrary shapes where the coefficient c varies with the geometry of the body but is always of order unity (Friedlander 1957, Clift et al. 1978, Leal 1992). For the intermediate region of Péclet numbers, numerical results for spheroids were published by Masliyah & Epstein (1972). These correlations between *Sh* and *Pe* are only valid, however, for simple, smooth shapes without spines, horns and sharp corners (Leal 1992). Spines and horns are common among phytoplankton and may have important roles in altering flow fields around cells and thus fluxes to cells. It is commonly thought that eddy formation does not occur at $Re < 1$, but eddy formation has been demonstrated within a corner formed by two intersecting planes in creeping flow (Jeffrey & Sherwood 1980). Eddies will reduce the contribution of advective transport since they will cause water to remain longer within that region before being replaced. These studies may have relevance to some diatoms such as *Thalassionema* and *Asterionella* species that form star-shaped colonies or zigzag bands of colonies. Also pertinent to sinking chains is the study by Dorrepaal & O'Neill (1979) for the case of uniform Stokes' flow past two parallel, separated cylinders with flow direction perpendicular to the line joining their centres. They found that fluid always moves through the gap separating the two cylinders but that eddies form for gap widths smaller than 0.0446 times the cylinder radius. This observation is also relevant to the study of suspension feeders. Interestingly, in the evolution of chain formation in planktonic diatoms, colonies show a tendency to become more and more disjointed, while conserving appreciable stiffness (Beklemishev 1959). The most straightforward interpretation is that cells thereby avoid each other's depleted diffusional boundary layers and allow flow between cells.

Observations: nutrient uptake by motile cells in stagnant water

We know of remarkably few attempts to test these theories even in the engineering context. Empirical data obtained from electrochemical measurements for large values of *Pe* are in good agreement (within 4%) with Equation 17 (Kutateladze et al. 1982). We are not aware of similar experiments for intermediate and low Péclet numbers. Experiments with live organisms are even harder to conduct. While batch cultures are often maintained without agitation, the parameters needed to test the theory are not measured. Furthermore, it is a fallacy to regard unstirred vessels as stagnant. It is difficult to avoid circulation due to thermal gradients without deliberate water jacketing and prevention of evaporation, as anyone who has tried to measure slow settling velocities knows. Conversely, without stirring, cultures can become inhomogeneous both in cell concentrations and in nutrient concentrations. It is thus difficult to make valid assumptions about velocity and concentration fields in typical batch culture.

Nutrient fluxes on the scale of interest are difficult to detect. Therefore a common approach is to measure nutrient uptake by cells. Nutrient uptake is sensitive to physiological state of the cell and depends on conditions under which cells have been grown (Dortch et al. 1991). It represents a lower bound on flux to the cell and reflects an increase in flux quantitatively only so long as the uptake system is not saturated. Moreover, experimental errors may often be comparable in magnitude to the predicted enhancement of flux, especially if test organisms are very small.

Testing the contribution of swimming and sinking to flux in laboratory settings is subject to added logistical difficulties. Canelli & Fuhs (1976) attempted to examine the effect of

sinking on phosphorous uptake by the diatom *Thalassiosira fluviatilis* by drawing an analogy with cells held on a filter through which a constant volumetric flow rate of nutrient medium passed. The flow regime in this experiment cannot be described by Equations 16–18 and is more analogous to the flow of pore waters through sediments (i.e. may be more relevant for diatoms experiencing pressure-driven flows in the benthos or in planktonic particle aggregates). This study demonstrated an effect of advection, but its results cannot be related quantitatively to natural fluid motions on single cells in the water column.

Mass transfer to cells in steady shear flow

Theory

Non-motile cells in steady shear flow

Another flow field that a cell can encounter is steady shear. Steady shear flow is associated with viscous dissipation of small-scale turbulence and with flows created in shear tanks to study nutrient uptake by phytoplankton and bacteria. It also holds for viscous sublayers (e.g. bottom boundary layers). By definition, a steady shear flow is one in which $\partial U/\partial t = 0$ and

$$\mathbf{U(X)} = \mathbf{V} + \boldsymbol{GX}\,, \qquad \text{(Equ. 23)}$$

where $\mathbf{V}$ is the mean velocity vector, $\boldsymbol{G}=\nabla\mathbf{U}$ is the velocity gradient tensor ($G_{ij}=\partial U_i/\partial X_j$) and $\boldsymbol{X}$ is a position vector (we use standard tensor notation, e.g. Spiegel 1959). From the point of view of a non-swimming, non-sinking planktonic osmotroph, only the relative velocity component ($\boldsymbol{GX}$) is important. The velocity gradient ($\boldsymbol{G}$) can be decomposed into two components (Lighthill 1986), rotation rate ($\boldsymbol{\Omega}=\Omega_{ij}= 0.5(\partial U_i/\partial X_j-\partial U_j/\partial X_i)$) and rate of strain ($\mathbf{E}=E_{ij}=0.5(\partial U_i/\partial X_j+\partial U_j/\partial X_i)$):

$$\mathbf{G} = \boldsymbol{\Omega} + \mathbf{E}\,. \qquad \text{(Equ. 24)}$$

Unlike self-induced rotation, which is typically parallel to the direction of motion, as in the case of dinoflagellates swimming in helical wave motion, a shear flow causes the cell to rotate with an axis of rotation perpendicular to the velocity gradient (Fig. 4). While the straining motion of the flow acts to reduce the thickness of the boundary layer around the cell and thus to enhance the flux of nutrients (Fig. 1), rotation will weaken the effect of advection on nutrient flux because it acts to close streamlines, making them less effective in carrying nutrients to the cell (Batchelor 1979). Thus in a shear flow, the net contribution of advection will be determined by the ratio $|\boldsymbol{\Omega}| / |\mathbf{E}|$.

The governing equation for the concentration distribution around a cell in a linear, steady shear flow is again the dimensionless Equation 11 with the boundary conditions (12, 13), where $\boldsymbol{U}^*$ is the nondimensional velocity field of the shear flow. We define the characteristic velocity of the shear flow ($|U|_{shear}$), and hence the Péclet number of the cell, in terms of the shear rate E:

$$|U|_{shear} \equiv EL_c \text{ and} \qquad \text{(Equ. 25)}$$

$$Pe_{shear} \equiv \frac{EL_c^2}{D}\,, \qquad \text{(Equ. 26)}$$

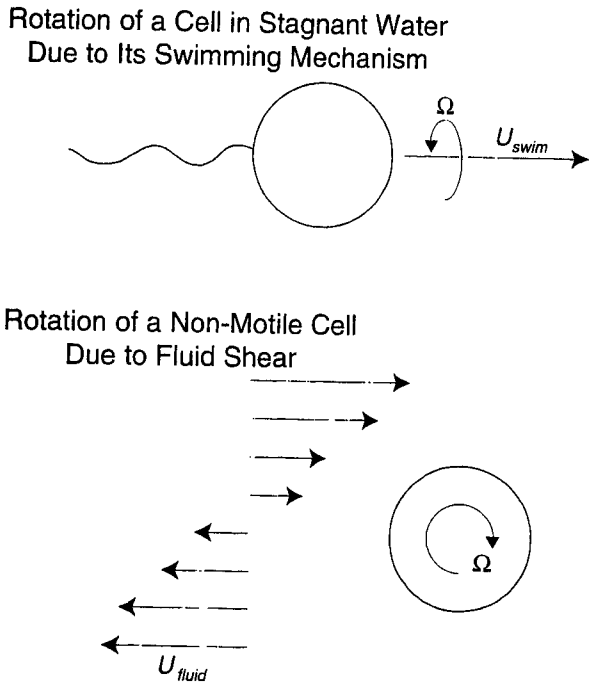

Figure 4 Rotation of cells due to swimming and fluid shear. While cells swimming with a flagellum in a helical wave motion tend to rotate so that their axis of rotation parallel the direction of translation, non-motile cells suspended in a simple shear flow rotate with their axis of rotation perpendicular to the flow direction. In the latter case rotation will weaken the effect of shearing on nutrient flux relative to a non-rotating cell in shear. Passive, flow-induced rotation causes streamlines around the cell to curve or even close, making them less effective in carrying nutrients.

where the shear rate is defined as

$$E \equiv |\mathbf{E}| = \left(E_{ij}E_{ij}\right)^{\frac{1}{2}}. \qquad \text{(Equ. 27)}$$

The dimensions of a shear rate [T^{-1}] can be easily intuited by noting that a shear is a difference in velocity [LT^{-1}] across a distance [L]; division eliminates the length scale and yields the rate. Its magnitude can be estimated from measurements of kinetic energy dissipation rate of the flow (ε, [L^2 T^{-3}]) since for any given shear flow

$$\varepsilon = 2\nu E_{ij}E_{ij}, \qquad \text{(Equ. 28)}$$

and thus

$$E = \left(\frac{\varepsilon}{2\nu}\right)^{\frac{1}{2}} = 0.71\left(\frac{\varepsilon}{\nu}\right)^{\frac{1}{2}}, \qquad \text{(Equ. 29)}$$

where ν is the kinematic viscosity (L^2 T^{-1}). The characteristic length scale (L_c) is taken again to be the cell radius (r_0).

The simplest shear flow is steady with all components of the rate of strain tensor (E_{ij})

equal to zero except $E_{12} = E_{21} = \Omega = (\gamma/\sqrt{2})$ (e.g. $\mathbf{U} = (\gamma y, 0, 0)$; Leal 1992). This flow is not applicable directly to the upper mixed layer in the field but is of interest because many laboratory experiments on the effects of shear on planktonic micro-organisms have been performed in Couette devices that produce such shear flows and because laminar sublayers of the boundary layers above the sea bed and surrounding objects in the sea do have this structure. A correlation between *Sh* and *Pe* for one-dimensional, steady shear flow was obtained by Frankel & Acrivos (1968) (see also Leal 1992) for $Pe \ll 1$:

$$Sh = 1 + 0.26\left(\frac{r_0^2\gamma}{D}\right)^{\frac{1}{2}} + o\left(Pe_{shear}^{\frac{1}{2}}\right). \qquad \text{(Equ. 30)}$$

After transforming to our previously defined E and Pe_{shear},

$$Sh = 1 + 0.31Pe_{shear}^{\frac{1}{2}} + o\left(Pe_{shear}^{\frac{1}{2}}\right). \qquad \text{(Equ. 31)}$$

Because the axis of flow-induced rotation is perpendicular to flow direction, at high Péclet number – when rotation is strong and closed streamlines are formed around the cell – *Sh* asymptotically approaches 4.5 as $Pe \to \infty$ (Frankel & Acrivos 1968).

In nature, however, flow experienced by very small cells is a three-dimensional linear shear field whose orientation relative to the cell shifts continually. Solutions for mass transfer in more general, steady, linear shear were derived by Batchelor (1979) for limiting cases. For $Pe \ll 1$ and any pure straining motion ($\Omega = 0$):

$$Sh = 1 + 0.36Pe_{shear}^{\frac{1}{2}}, \qquad \text{(Equ. 32)}$$

where the numerical coefficient is accurate within 3%. The essence of pure straining motion at the scale of the cell is that the net hydrodynamic force acting on the cell is zero, i.e. there is relative motion between the cell surface and the fluid but there is no net force that causes the cell to rotate or translate. When the ratio $|\Omega| / |\mathbf{E}| \leq 1$ and $Pe \ll 1$,

$$Sh = 1 + 0.34Pe_{shear}^{\frac{1}{2}}, \qquad \text{(Equ. 33)}$$

where the error in the numerical coefficient does not exceed 10%. When the ratio $|\Omega| / |\mathbf{E}| > 1$ and $Pe \ll 1$, only shear rate in the direction parallel to the axis of rotation (E_ω) contributes to advective flux:

$$Sh = 1 + 0.4\left(\frac{r_0^2|E_\omega|}{D}\right)^{\frac{1}{2}} \approx 1 + 0.23Pe_{shear}^{\frac{1}{2}}, \qquad \text{(Equ. 34)}$$

where we use Batchelor's (1979) assumption that $E_\omega^2 \approx E^2/9$. This relation stems from the observation that there are nine terms like E_ω^2 in the expression for E^2. Thus it should provide a lower bound on *Sh*.

For $Pe \gg 1$ and pure straining motion, the relation between *Sh* and *Pe* becomes (within an error of $\leq 1\%$)

$$Sh = 0.9Pe_{shear}^{\frac{1}{3}}. \qquad \text{(Equ. 35)}$$

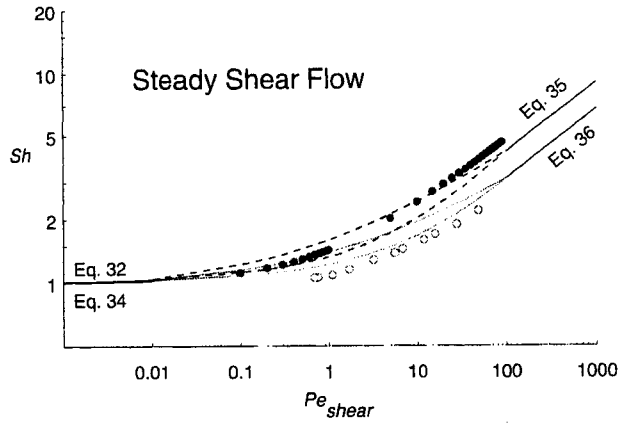

Figure 5 Sherwood number (*Sh*) as a function of Péclet number (*Pe*) for non-motile cells suspended in a steady, linear shear. Solid lines are based on analytic solutions derived for $Pe \ll 1$ and $Pe \gg 1$. Equations 32 and 34 were derived for cells in linear shear in the absence of rotation and in the presence of strong rotation, respectively, for $Pe \ll 1$ (Batchelor 1979). At small values of *Pe* molecular diffusion is the governing transport mechanism, and rotation will have no significant inhibitory effect on advective flux. At large *Pe*, however, strong rotation partially suppresses advective flux as indicated by the difference between the results of Equation 35, which was derived for the non-rotating case and Equation 36, which was derived for strong rotation (both by Batchelor 1979). *Sh* values for $0.1 < Pe < 90$ were obtained numerically for the case of uniaxial, extensional flow (filled circles; Appendix II). The curve fitted to the numerical values (for $0.1 < Pe < 90$) is of the form $Sh = 0.63Pe^{0.4} + 0.82$ (not shown). Based on the scheme used for the model, we estimate the absolute error in our numerical solution for small *Pe* to be < 0.005. For large *Pe* the estimated error is predicted to be $< 1\%$ of *Sh*. We are not aware of any general analytic or numerical solutions for the region $0.01 < Pe < 100$, in which many marine osmotrophs fall. Therefore, estimates of *Sh* for that region were obtained by interpolation for each of the two cases (i.e. pure straining motion and shearing motion in the presence of strong rotation). Interpolations assume a function of the form $Sh = a + bPe^c$, where c for each case falls between the limits of its values for the interpolation through the low-*Pe* solution at $Pe = 0.01$ ($Sh = 1.004 + 0.32Pe^{1/2}$ in the absence of rotation (lower dashed line); $Sh = 1.002 + 0.21Pe^{1/2}$ in the presence of strong rotation (lower dotted line)) and the high *Pe* solution at $Pe = 100$ ($Sh = 0.883 + 0.71Pe^{1/3}$ in the absence of rotation (upper dashed line); $Sh = 0.921 + 0.47Pe^{1/3}$ in the presence of rotation (upper dotted line)). The region between these two interpolation limits is marked in gray. Open circles denote the empirical data of Purcell (1978), who studied heat transport from spheres in a steady, two-dimensional, pure straining motion (i.e. no rotation). Explanations for the discrepancies between the analytical results, our numerical model for high *Pe* values and Purcell's results are given in the text.

For $Pe \gg 1$ when rotation and strain both act,

$$Sh = 0.97\left(\frac{r_0^2|E_\omega|}{D}\right)^{\frac{1}{3}} \approx 0.67Pe_{shear}^{\frac{1}{3}}, \qquad \text{(Equ. 36)}$$

again making the same assumption about the relation between E_ω and E. Equations 35 and 36 demonstrate the relative reduction in mass transfer owing to rotation at high *Pe* (Fig. 5). We

are not aware of published analytic or numeric solutions for intermediate values of Pe; therefore for the region $0.01 < Pe < 100$ our plotted values for Sh were obtained by interpolation through the low-Pe solution at $Pe = 0.01$ and the high-Pe solution at $Pe = 100$ (Fig. 5). Our interpolations assume conservative functional form, i.e. $Sh = a + bPe^c$, where c falls between the limits of its values for high and low Pe and a and b are chosen to fit the two endpoints. We also obtained Sh values for the region $0.1 < Pe < 90$ by solving the problem numerically for the case of pure straining motion (Figure 5; Appendix II). When rotation is not zero, the problem becomes three-dimensional, and we do not attempt even numerical solution here. For $0.1 < Pe < 10$ our numerical results fall in the region between the two interpolation limits obtained for purely straining flow (Fig. 5). For larger Pe, Sh values predicted by our numerical model are higher than the upper interpolation limit. One explanation for this discrepancy is that Equation 35 provides only a first-order approximation for the increase in flux. We are not aware of higher-order expansions for the case of shear flow but we expect that such solutions will include terms of order smaller than $Pe^{1/3}$ (e.g. a constant, as in the case of the higher-order expansion for uniform flow (Equation 17)). A function of the form $Sh = 0.9Pe^{1/3} + c$ was fitted to our numerical results in the region $50 < Pe < 90$, suggesting that a constant of 0.56 should be added to Equation 35.

Laboratory experiments

Validation of the theory in an engineering context

Measurements of mass transfer in shear flow are consistent with theory for large Pe (i.e. $Sh \propto Pe^{1/3}$; Kutateladze et al. 1982). The value of the proportionality constant suggested by the data, however, is 10% smaller than suggested by Equation 35. This discrepancy is not surprising since the experimental setup (fixed sphere in a shear flow) did not exactly mimic the case of a sphere suspended in an ambient shear flow for which Equation 35 was derived (Kutateladze et al. 1982).

Empirical results that include the region of intermediate Pe (Fig. 5) were provided by Purcell (1978), who performed an experiment to study the transport of heat from a spherical particle suspended in a steady, two-dimensional, purely straining shear (i.e. no rotation). The sphere in his experiments was immersed in a fluid of high viscosity, and the velocity field was established by four counter-rotating cylinders. From the temperature difference between the surface of the heated sphere and the fluid, he obtained a relationship between heat transfer and shear. Purcell's results indicate that, for $Pe \ll 1$, Sh is proportional to Pe^2. This disagreement between theory and experimental results may be the result of the sensitivity of mass transfer at small Pe to flow geometry at large distances from the body. Shear in Purcell's experiment was disturbed by boundaries about eight radii from the sphere, while the analytic solution considers an unbounded flow field (Batchelor 1979). Nevertheless, Purcell's results have been used by several authors to predict the effect of turbulence on fluxes of nutrients to suspended osmotrophs (Lazier & Mann 1989; Jumars et al. 1993). We (Jumars et al. 1993) compounded confusion by finding good fit of Purcell's (1978) data to an inappropriate equation, i.e. one derived for Stokes' flow past a sphere (Clift et al. 1978; their equation 3–49), before we had encountered the full diversity of low-Re flow regimes of interest in questions of nutrient flux to and from cells. We further failed to transform Clift et al.'s equation to our definitions of Pe and Sh.

Nutrient uptake in steady shear

Very few experimental data are available for testing this theory in an oceanographic context. Logan & Dettmer (1989) investigated the effect of a laminar shear on leucine uptake by bacteria for shear rates ranging from $E = 0 s^{-1}$ to $E \approx 56 s^{-1}$ ($0 \leq \gamma < 80 s^{-1}$), although for shear rates of $E > 35 s^{-1}$ the fluid became unstable and could no longer be considered laminar. Shear rates were estimated from simple engineering relations for stirred vessels (Logan & Dettmer 1989, Van Duuren 1968). The model for simple, steady, shear flow (Equation 31) predicts an increase of 3% in leucine flux ($D_{leucine} = 7 \times 10^{-6} cm^2 s^{-1}$) for a cell with a radius of 0.45 μm exposed to a shear rate of $35 s^{-1}$. Uptake by bacteria exposed to shear, however, did not increase compared with uptake by bacteria suspended in stagnant fluid. Instead, high shear rates seemed to impair leucine uptake. Shear rates used in this experiment were far above any typical values encountered by bacteria in the ocean (shear rates in the mixed layer varying from 0.01 to $1 s^{-1}$), and the observed inhibition of uptake by shear may have resulted from stress or even mechanical damage.

In a later study, Logan & Kirchman (1991) investigated the effect of fluid shear ($E < 1.5 s^{-1}$ for $\gamma \leq 2.1 s^{-1}$) on leucine uptake by natural assemblages of marine bacteria. Their results showed no significant (less than 10% departure from unstirred vessels) enhancement of leucine uptake at shear rates $0 < E < 1$. Their results agree with the model prediction (Equation 31) that for organisms of typical bacterial size laminar shear is ineffective at increasing uptake of molecules with a diffusion coefficient of the order 10^{-5}–$10^{-6} cm^2 s^{-1}$. Their experimental error (standard deviation being 5% to 32% of the mean), however, is larger than the increase in the flux predicted by Equation 31; therefore, the experiment cannot provide a strong test of the theory.

Few experimental data are available for larger organisms. Pasciak & Gavis (1975) studied NO_3^- uptake by a cylindrical diatom (*Ditylum brightwellii*), with an equivalent spherical radius of about 41 μm, when suspended in a controlled shear tank (i.e. Couette device) at $0 < E < 8.5 s^{-1}$ ($0 < \gamma < 12 s^{-1}$). Their fitted curve suggests a Michaelis–Menten type relationship between relative uptake and shear rate with a maximal increase in relative uptake (*c.* 9%) at a shear rate $E \approx 5 s^{-1}$. As mentioned above, shear rates larger than $1 s^{-1}$ are probably higher than encountered in nature. For more realistic shear rates they observed 2% increase in relative uptake at a shear rate $E \approx 0.35 s^{-1}$. The simple shear model (Equation 31) predicts an increase of 24% in the *total flux* of NO_3^- to the cell surface ($D_{NO_3} = 1.9 \times 10^{-5} cm^2 s^{-1}$, Li & Gregory 1974). The offset between experimental results and theory may result from some combination of greater saturation of the uptake system under conditions of shear (predicted flux, therefore, over-estimating uptake), failure of the theory to include the shape effects of non-spherical cells and experimental error, whose magnitude was not provided. In summary, there are no published data that show statistically significant departure from model predictions for simple shear flow, but no strong tests have been performed.

Mass transfer to cells in turbulent water

Non-motile cells in turbulent flow

Turbulence acts to mix water and increase rates of momentum, heat and mass transfer. Turbulence is strongly intermittent in amplitude, space and time and is always dissipative.

Kinetic energy is transferred from large, turbulent eddies into smaller ones and then is dissipated as heat by viscous friction. The length scale of the smallest eddies associated with the turbulent flow is known as the Kolmogorov length scale, η (Tennekes & Lumley 1972),

$$\eta = \left(\frac{\nu^3}{\varepsilon}\right)^{\frac{1}{4}}, \qquad \text{(Equ. 37)}$$

where ε is the turbulent kinetic energy dissipation rate [$L^2\ T^{-3}$] and ν is the kinematic viscosity (approximately $0.01\,cm^2s^{-2}$). Organized rotational motions of the fluid in the absence of particles are thought not to exist below this scale. Typical values of the energy dissipation rate in the oceanic upper mixed layer range from 10^{-2} to $10^{-5}\,cm^2s^{-3}$ (Oakey & Elliott 1982, Gargett 1989, Brainerd & Gregg 1993). Thus, in the upper mixed layer the Kolmogorov scale is on the order of 1–6mm. Above the Kolmogorov scale, the flow is turbulent (i.e. irregular and dominated by inertial forces), while below it viscosity dominates, resulting in laminar shear (Table 4). Another feature of the turbulent flow field below the Kolmogorov length scale is that the statistical state of small-scale fluctuations is considered to be homogeneous, isotropic and practically steady (Monin & Yaglom 1975).

Table 4 Characteristic flow fields at large distance from the cell, dominant transport mechanisms and proposed solutions for nutrient tranfer to cells.

Scalings	Flow regimes	Dominant transport mechanisms	Relevant equations
$Re \ll 1$, $r_0 \ll \eta_b$, $Pe \ll 1$	Steady, laminar shear	Molecular diffusion	Equation 48
$Re \ll 1$, $r_0 \approx \eta_b$, $Pe \approx 1$	Steady, laminar shear	Molecular diffusion and laminar advection	No solution available (see Fig. 6)
$Re \ll 1$, $\eta_b < r_0 < \eta$, $Pe > 1$	Statistically steady, laminar shear	Laminar advection	No solution available (see Fig. 6)
$Re < 1$, $r_0 \leq \eta$, $Pe \gg 1$	Statistically steady, laminar shear	Laminar advection	Equation 49
$Re \approx 1$, $r_0 \approx \eta$, $Pe \gg 1$	Transitional flow (between laminar and turbulent)	Laminar and turbulent	Outside the scope of this review. Do not attempt to apply our equations
$Re > 1$, $r_0 > \eta$, $Pe \gg 1$	Turbulence	Turbulent advection	

Hence, ambient flow in the vicinity of phytoplankton and bacteria (except for large chains of diatoms and filamentous cyanobacteria) can be very well approximated as a linear shear field. Based on published field measurements of micro-structure Lazier & Mann (1989) suggested that the smallest energy-containing eddies have a length scale larger by a factor of 5–10 than the Kolmogorov scale and proposed that a coefficient of $c.$ 10 should be used with the right side of Equation 37. A major limitation in addressing the role of turbulence in the nutrition of planktonic osmotrophs is the rarity of flow measurements at microscopic levels. Current knowledge of the flow regime in the vicinity of planktonic micro-organisms is based solely on theoretical arguments and on measurements of flow at macroscopic levels. Accepting Equation 37 as representing the size of the eddies below which the flow field can be well approximated as a laminar shear field will not result in a large error, however, so long as the cells in question are much smaller than η produced by Equation 37.

A second relevant length scale addresses the smallest variations in the ambient concentration field. It was introduced by Batchelor (1952) but has seen far less frequent application than Equation 37:

$$\eta_b = \left(\frac{\nu D^2}{\varepsilon}\right)^{\frac{1}{4}} . \qquad \text{(Equ. 38)}$$

This length scale is smaller than the Kolmogorov scale because diffusion coefficients are smaller for molecules such as nutrients [$O(10^{-5}cm^2s^{-1})$] than for momentum [$O(10^{-2}cm^2s^{-1})$]; mass transfer requires displacement of molecules, while momentum can be transferred in successive molecular collisions without as much net displacement. This length scale separates the region in which the principal transport mechanism is shearing motion versus diffusion (Table 4). At length scales larger than η_b but smaller than η, temporal changes of the velocity field are slower than the Kolmogorov time scale of $(\nu/\varepsilon)^{1/2}$, and the flow is considered to be statistically steady (Table 4). Below this scale, molecular diffusion dominates transport and has a characteristic time scale L_c^2/D (where L_c is a characteristic length scale). If we choose L_c to be $(\nu D^2/\varepsilon)^{1/4}$, then the characteristic timescale of diffusion becomes $(\nu/\varepsilon)^{1/2}$. This result implies that below η_b diffusional adjustment is faster than variations in the flow, and the flow can therefore be approximated as steady shear. In the mixed layer, η_b may range between 32μm and 180μm (assuming a kinetic energy dissipation rate of 10^{-2} to 10^{-5} cm^2 s^{-3} and $D = 1 \times 10^{-5}$).

A turbulent flow field is often decomposed into its mean (e.g. over an ensemble of measurements) and fluctuating components as

$$\mathbf{U} = \overline{U} + u' . \qquad \text{(Equ. 39)}$$

The strain tensor can be decomposed similarly as

$$\mathbf{E} = \overline{E} + e' . \qquad \text{(Equ. 40)}$$

Since in a turbulent flow

$$\overline{\overline{E}_{ij}\overline{E}_{ij}} \ll \overline{e_{ij}e_{ij}} \qquad \text{(Equ. 41)}$$

(Tennekes & Lumley 1989), the relation between shear rate and kinetic energy dissipation rate is effectively

$$\varepsilon = 2\nu\overline{e_{ij}e_{ij}} . \qquad \text{(Equ. 42)}$$

For isotropic turbulence ($e_{ii} = e_{jj}$, $e_{ij} = e_{kl}$, $i \neq j$, $k \neq l$, and the mean rate of extension equals zero), only one component of the strain tensor is needed to describe the relationship between ε and shear rate. The relationship between the r.m.s rate of extension in a fixed direction and ε was given by Taylor (1935),

$$\left(\overline{e_{11}^2}\right)^{\frac{1}{2}} = 0.26\left(\frac{\varepsilon}{\nu}\right)^{\frac{1}{2}} \qquad \text{(Equ. 43)}$$

and,

$$\left(\overline{e_{11}^2}\right) = \frac{1}{2}\left(\overline{e_{12}^2}\right) . \qquad \text{(Equ. 44)}$$

The local axis of rotation, however, changes over time. A relation between the mean rate of extension parallel to the local axis of rotation ($\langle E_\omega \rangle$) and ε was given by Batchelor (1980),

$$\langle E_\omega \rangle = \frac{7}{6\sqrt{15}} S\left(\frac{\varepsilon}{\nu}\right)^{\frac{1}{2}} , \qquad \text{(Equ. 45)}$$

where S is a skewness factor of the rate of extension in a fixed direction. Its values range from 0.3 to 1, based on measurements in various turbulent flows and over a wide range of Reynolds numbers (Batchelor 1980). Since the measures for oceanic turbulence are ε and ν, we define the characteristic velocity and hence Pe in terms of those parameters:

$$U_{turbulence} \equiv \left(\frac{\varepsilon}{\nu}\right)^{\frac{1}{2}} r_0 \qquad \text{(Equ. 46)}$$

and

$$Pe_{turbulence} \equiv \frac{r_0^2}{D}\left(\frac{\varepsilon}{\nu}\right)^{\frac{1}{2}}. \qquad \text{(Equ. 47)}$$

We are not aware of solutions for mass transfer to particles suspended in turbulent flow for small or intermediate values of Pe. For cells smaller than η_b (which by definition means $Pe < 1$), however, the flow can be assumed to be steady. In addition, since in isotropic turbulence the ratio between $E_{turbulence}$ and $\Omega_{turbulence}$ is of order 1, Equation 33 (steady shear flow at $Pe \ll 1$, where $E/\Omega \leq 1$) can be used to describe mass transfer to cells suspended in turbulent water. After replacing Pe_{shear} with $Pe_{turbulence}$, using Equation 42 to convert E $(=\overline{e_{ij}e_{ij}})$ to terms of ε/ν, Equation 33 becomes

$$Sh = 1 + 0.29 Pe_{turbulence}^{\frac{1}{2}}. \qquad \text{(Equ. 48)}$$

For cells larger than η_b but smaller than η, Equation 36 (for $Pe \gg 1$) can be used after converting E_ω to terms of ε and ν, according to Equation 45 (Batchelor 1980). Batchelor (1980) used $S = 0.6$ to solve for mass transfer to spherical particles in statistically steady (but not necessarily homogeneous), turbulent flow:

$$Sh = 0.55 Pe_{turbulence}^{\frac{1}{3}}. \qquad \text{(Equ. 49)}$$

The leading coefficient in this equation will vary by 20% depending on the choice of S. We caution that varying definitions of shear rate (and hence Pe) have been used. In several

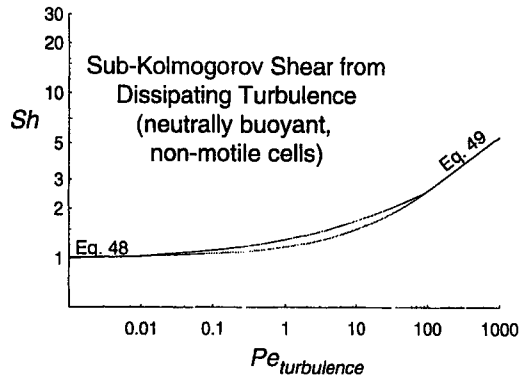

Figure 6 Sherwood number (Sh) as a function of Péclet number (Pe) for non-motile cells suspended in turbulent water. For $Pe \ll 1$ (i.e. cells smaller than η_b) we used Equation 48 for steady shear flow, and for $Pe \gg 1$ we used Equation 49, which was derived for statistically steady shear flow. For $0.01 < Pe < 100$, Sh values were obtained by interpolation (gray area) as described in Figure 5 where the lower limit for interpolation is given by $Sh = 1.014 + 0.15Pe^{1/2}$ and the upper limit is given by the line $Sh = 0.955 + 0.344Pe^{1/3}$.

studies, a less rigorously defined shear rate was related to ε by an arbitrary leading coefficient of 0.5 (e.g. Bowen et al. 1993, Jumars et al. 1993). In the absence of analytic or numeric solutions for intermediate values of *Pe*, *Sh* values used here for the region $0.01 < Pe < 100$ were obtained by interpolation (Fig. 6).

Application to the ocean

Turbulent kinetic energy dissipation rate (ε) in the ocean shows great variability in both space and time, making the choice of a representative value of the shear experienced by cells challenging and maybe unwise. Within the mixed layer, successive estimates of ε differ by an order of magnitude (Shay & Gregg 1986). Turbulent kinetic energy dissipation rates are high at the surface and decay with depth, often decreasing by an order of magnitude per meter (Brainerd & Gregg 1993). Dissipation rates vary daily, seasonally and annually. Furthermore, in the near-surface zone, values of ε obtained a few hours apart may differ by three orders of magnitude (Brainerd & Gregg 1993). Turbulence can be beneficial if cells are suspended in high shear long enough to allow appreciable enhancement of nutrient flux. Since published values of estimated turbulent kinetic energy dissipation rates are time averaged, one must know the distribution function of ε in order to estimate the fraction of the time that a cell is exposed to a given shear. The distribution function of dissipation estimates drawn from surface mixed layers is nearly lognormal (Osborn & Lueck 1985, but see Yamazaki & Lueck 1992) and is parameterized by $\bar{x}_{\ln\varepsilon}$ and $s^2_{\ln\varepsilon}$, the mean and the variance of lnε. The latter is a measure of the intermittency of the turbulence. For example, taking a value of the variance in the upper mixed layer $s^2_{\ln\varepsilon} = 1.5$ (Baker & Gibson 1987), the dissipation rate will have a value equal to or smaller than the mean 73% of the time (Shimeta 1993). Because of the strong intermittency of turbulence, its effect on flux will vary greatly in space and time and will probably be more significant in coastal zones, where turbulence is more intense, than in the open ocean.

If we assume a characteristic value of ε in the surface layer to be $10^{-2}\text{cm}^2\text{s}^{-3}$, theory suggests that turbulence in the ocean will favour large-celled competitors. The critical cell size for 50% increase in the flux ($D = 1\times10^{-5}\text{cm}^2\text{s}^{-1}$) at this dissipation rate ranges between 63–100μm (Table 2). Planktonic bacteria (other than filamentous blue-greens) and small flagellates are well below this limit, while large cells, chains and colonies are above it. These calculations indicate a stronger effect of turbulence than previously supposed. Assuming a diffusion coefficient $D = 2 \times 10^{-5}\ \text{cm}^2\ \text{s}^{-1}$, Lazier & Mann (1989) calculated, based on the experimental results of Purcell (1978), an increase in the flux of only 2% for cells 50μm in radius in the presence of strong turbulence ($\varepsilon = 10^{-2}\text{cm}^2\text{sec}^{-3}$) – while the model we use suggests an increase a full order of magnitude greater (18–32%; Fig. 6).

The behaviour of cells in turbulent flow is not well known but is likely to vary strongly with shape. Since large cells, chains and colonies are the ones expected to benefit most from turbulence, a better understanding of their behaviour in turbulent flow is needed. Whether chains are straight, bent, rigid or flexible will affect their behaviour in shear flow and hence their nutrient fluxes and competitive abilities. For instance, the period of rotation of permanently bent, threadlike particles is appreciably lower than that of straight particles (Forgacs & Mason 1959). If this disparity holds in the pelagic environment, one may expect straight chains to experience reduced flux compared to bent chains. In both theoretical and empirical results Van de Ven & Mason (1976) showed that the behaviour of chains of equal-sized

spheres in simple shear flow depends on whether the units in the chain touch each other. A straight chain of touching units will rotate as a rigid body when exposed to shear while a chain of non-touching spheres will change length periodically with their orientation. Curved chains that are not rigid will bend. Although the units in chains of non-touching spheres were not attached directly to each other by means of thin, flexible threads (as in the case of some diatom species), but were held together by means of electrostatic and van der Waals forces, and although the results of their study are limited to Poiseuille flow and short chains (up to 5 units), they are intriguing in the light of the diverse morphologies of chains observed in nature and the evolutionary trend in diatom chain formation toward non-touching cells. Details of spacing within chains will alter the way that turbulence and bending "pump" nutrient-replete water between the cells of chains.

There are no measurements of nutrient uptake by cells suspended in controlled turbulence that can be tested against this theory. Results from experiments done in bottles placed on shaker tables and plankton wheels or stirred with stir bars do not provide strong insight about turbulence effects since the nature of the flows and the magnitudes of shear are neither well quantified nor related to nature. Savidge (1981), who investigated the effect of turbulence on uptake rate of phosphate and nitrate by the diatom *Phaeodactylum tricornutum*, used an oscillating grid to produce turbulence. Unfortunately, neither shear rate nor energy dissipation rate was determined, and no information was provided about sizes of cells or the magnitude of experimental error. Oscillating-grid turbulence shows extreme spatial variability, the dissipation rate falling off as the fourth power of distance from the grid (Brumley & Jirka 1987). Therefore, no quantitative conclusions can be drawn from this experiment. Better indication at high *Pe* comes from chemical engineering experiments on dissolution rates of particles in turbulent, stirred flows. These data have been reviewed and summarized by Batchelor (1980), who found good fit to the predictions.

Translational motion in turbulent water

Swimming and sinking in turbulent water

The solutions presented so far for mass transfer in the presence of turbulence-induced shear assumed that the cells were suspended without translation in turbulent water. In the real ocean, however, cells in turbulent water may swim or sink. The resultant flow field can be expressed as a superposition of steady translational motion and shear (Batchelor 1980). Total nutrient transfer to motile cells, for large *Pe*, becomes (Batchelor 1980):

$$Sh = \alpha\left[2.25\left(r\frac{U_{s^*}}{D}\right)^2 + 5.1S^2\left(\frac{r^2}{D}(\varepsilon/\nu)^{\frac{1}{2}}\right)^2\right]^{\frac{1}{6}} \qquad \text{(Equ. 50)}$$

The coefficient α depends on the ratio $5r_0e_{11}/U_{s^*}$ (where the asterisk indicates that only the component of the swimming or sinking velocity parallel to the axis of rotation is used. It varies between 0.495 (when $5r_0e_{11}/U_{s^*} \rightarrow \infty$, i.e. pure shearing motion of Equation 49) and 0.545 (when $5r_0e_{11}/U_{s^*} = 0$, i.e. pure translational motion as given by the first-order approximation of Equation 17). As mentioned previously, if a cell is rotating and closed streamlines are formed, translational motion will contribute to the flux in proportion to the magnitude of its component in the direction parallel to the axis of rotation. If isotropic turbu-

lence is assumed, however, the cell is continually reoriented, and the mean value of the component of translational motion parallel to the axis of rotation equals zero. Thus in turbulent water, as soon as the shear-induced rotation rate reaches a critical magnitude ($\Omega = U_s Pe^{-1/3}/r_0$, where $Pe = r_0 U_s/D$), swimming or sinking will have no appreciable effect on transfer of nutrients (Batchelor 1980). Even if the swimming mechanism imparts rotation parallel to the instantaneous swimming direction, high turbulence intensities may overwhelm the rotational component and effectively randomize the direction of translation.

A common observation, both spatially and temporally, is that small, motile phytoplankton cells tend to predominate in stratified, calm, oligotrophic water while large cells (mainly diatoms) prevail in turbulent, nutrient-rich water (Margalef 1978, Malone 1980, Mann 1992). Dominance of flagellates in calm water is probably a result of their ability to increase nutrient uptake through swimming - both from reaching layers of higher nutrient concentration and within any particular nutrient concentration from relative motion. In turbulent water, on the other hand, dinoflagellates may not be able to maintain a rotational axis parallel to the direction of the swimming or to the direction of the shear flow; thus they will suffer a relative reduction in nutrient flux. Predicted critical velocities below which swimming is no longer effective in enhancing the flux are of the same order of magnitude as maximal swimming velocities measured for dinoflagellates (Figure 7). Thus swimming, especially for large dinoflagellate cells, may not contribute significantly to flux under natural turbulence. There is increasing evidence that dinoflagellates are sensitive to strong shear. Under conditions of vigorous turbulence cells may suffer mechanical damage. Loss of flagella, changes in swimming behaviour, and growth-rate inhibition have been observed for several species of dinoflagellates exposed to straining motion in the laboratory (Thomas & Gibson 1990 a, b, 1992, Berdalet 1992).

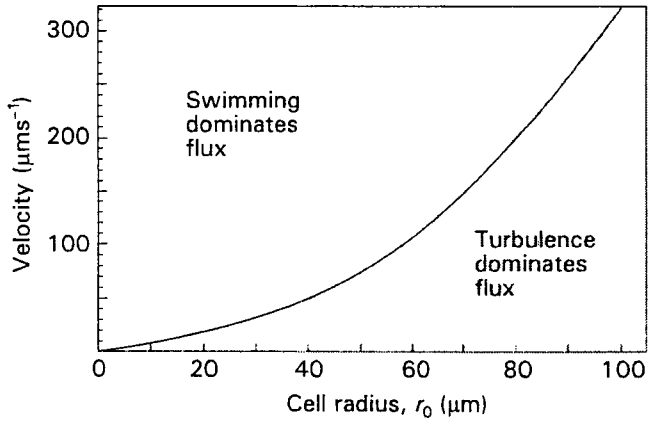

Figure 7 Critical velocities below which swimming or sinking cannot significantly affect the flux in turbulent water, as a function of cell size. Critical velocities were calculated based on Batchelor (1980) $U_{critical} = (r^2/\sqrt{D})(\varepsilon/\nu)^{3/4}$, with energy dissipation rate (ε) taken to be 1×10^{-2}cm^{2}s^{-3}, D to be 1×10^{-5}cm^{2}s^{-1} and ν to be 1×10^{-2}cm^{2}s^{-1}. For cells swimming or sinking more slowly (grey area under the solid line) turbulence so dominates the advective contribution to the flux that swimming or sinking is ineffectual.

Flow-induced translational motion

Cells and chains of sizes near the Kolmogorov scale may exhibit passive translational motion due to a lift force induced by curvature of the flow. Passive migration can increase total mass transfer because it adds an additional component of relative velocity between the cell and its surrounding water and facilitates encounter of cells with "new" water (i.e. changes C_∞). The idea of translational motion induced by turbulence stems from observations of the migration of rigid, neutrally buoyant particles in Poiseuille flow (a nonlinear shear flow with $\partial u_i/\partial x_j \neq$ constant, $i \neq j$, such as in pipes and blood vessels) at particle Reynolds numbers as low as 10^{-3} (Sergé & Silbergberg 1961, Karnis et al. 1963). Nonlinearity of the flow due to wall effects and small but non-negligible inertial forces (Goldsmith & Mason 1967, Leal 1980) impart the lift force that causes migration. Flexible particles show similar behaviour even at smaller Reynolds numbers as a result of lift due to shear deformation (Goldsmith & Mason 1961, Karnis et al. 1963). The direction of the migration of neutrally buoyant particles in Poiseuille flow is to the region of minimal shear, while the direction of migration of non-neutrally buoyant particles depends on whether the particles lead or lag the local undisturbed motion (Leal 1980). Since a similar phenomenon has also been predicted in unbounded flows (Saffman 1965a) it may be relevant for large cells in turbulent water.

To calculate the translational velocity that results from curvature of the flow, we assume a one-dimensional flow field of one Fourier component with the length scale of the smallest energetic eddy. This simplification is suitable for our purpose since the turbulent flow field is assumed to be isotropic. We assume a free-stream flow velocity,

$$U_{flow} = \vartheta \sin\left(\frac{2\pi y}{\eta}\right), \qquad \text{(Equ. 51)}$$

where ϑ is the Kolmogorov scale of velocity $((\varepsilon\nu)^{1/4})$, η is the Kolmogorov length scale, and y is the spatial variable. Transverse (to the streamline) velocity of the phytoplankter due to lift is (Saffman 1965a, b, McLaughlin 1991)

$$U_{transverse} = 0.343 \Delta U \sqrt{Re_{shear}}\,, \qquad \text{(Equ. 52)}$$

where Re_{shear} is the Reynolds number of the particle based on the turbulence-induced shear and is defined as

$$Re_{shear} \equiv \frac{r_0^2}{\nu}\left(\frac{\partial U_{flow}}{\partial y}\right). \qquad \text{(Equ. 53)}$$

Equation 52 is independent of rotation, and the error is of order $Re \ll 1$. ΔU is the relative velocity between the flow speed at the centre of the particle (when the particle is removed) and the speed of the particle. The difference in the flow velocity and the particle velocity arises from the nonlinearity of the shear flow. Equation 52 holds only when the cell is not motile or if Re based on its swimming or sinking velocity (Re_s) is much smaller than the square root of the cell Reynolds number based on shear velocity (Re_{shear}). McLaughlin (1991) expanded Saffman's analysis to cases in which $Re_s \geq \sqrt{Re_{shear}}$ and demonstrated that migration velocity increases as the ratio $\sqrt{Re_{shear}}/Re_s$ increases. If we assume a typical shear rate for strong turbulence to be *c.* 0.5 s^{-1}, for a cell 50 µm in radius Re_{shear} becomes $O(10^{-2})$. Re for sinking cells is typically smaller than 10^{-2} (Table 1), and Equation 52 can be used to

calculate the translational velocity due to flow curvature. *Re* for swimming cells can be larger, and the corrections to Equation 49 suggested by McLaughlin (1991, his table 1) should be used.

In our case, the r.m.s. relative velocity that arises from the curvature of the flow is the second term of the Taylor expansion for particle velocity:

$$\Delta U = \frac{r_0^2}{4}\left(\frac{2\pi}{\eta}\right)^2 \vartheta \qquad \text{(Equ. 54)}$$

Thus,
$$U_{transverse} = 3.4\vartheta\left(\frac{r_0}{\eta}\right)^2 \sqrt{Re_{shear}}\,, \qquad \text{(Equ. 55)}$$

or
$$\frac{U_{transverse}}{\vartheta} = \frac{3.4 r_0^3}{\eta^2}\sqrt{\frac{1}{\nu}\frac{\partial U_{flow}}{\partial y}}\,. \qquad \text{(Equ. 56)}$$

For an organism 50–100μm in radius in turbulent water with $\varepsilon = O(10^{-2})\,cm^2 s^{-3}$ the transverse velocity is about 10^{-2}–10^{-4} body lengths s^{-1}. The *direct* contribution of shear-induced lift to the advective flux will strongly depend on cell size and will become important only when cell size is of order η. Our calculations suggest that migration due to curvature of the flow is potentially important in laboratory experiments but is probably of limited relevance to the pelagic environment.

Conclusions and prospects

Nutrient fluxes to planktonic osmotrophs in the presence of fluid motion depend on three sets of physical characteristics: the flow regime, the size and shape of the cell and the diffusion coefficient of the nutrient of interest. Solutions for the advective contribution to flux clearly do not carry over from one flow regime to another. Careful attention should be given, therefore, when comparing theoretical results with experimental or field data. For example, theoretical predictions derived for a cell in three-dimensional, isotropic turbulence cannot be tested directly by experiments in Couette flow devices. Advective flux in a given flow field will also be affected by the behaviour of the cell, e.g. rotation or deformation of flexible chains. Direct observations of behaviours of cells in shear flows or even of behaviours of cells while sedimenting, however, are practically non-existent.

A recurring theme is the potential effect of rotation on flux for all but one orientation, i.e. rotation about an axis parallel to the flow. We are not aware of any measurements of the magnitude of the rotation effect at any *Pe*. It could be explored in stagnant water and linear shear with slight modification of the approach of Purcell (1978) and seems important to an understanding of the ecology of dinoflagellates in particular. A key question is whether dinoflagellates in the presence of steady shear of varying magnitudes or of even gentle turbulence can maintain a rotational orientation that does not hinder nutrient exchange. It seems likely, however, that dinoflagellates are ill suited for experimentation in the Couette devices that are typically used to mimic some turbulence effects. At low shears their tendencies to

swim in more or less straight lines will cause them to interact frequently with the walls, and at high *Pe* they should suffer reduced fluxes from rotation for any rotational orientation that is not perfectly aligned with the curved plane of shear.

The contribution of advection to nutrient flux will increase with cell size. For nutrients of small molecular sizes, such as nitrate, phosphate, glucose or individual amino acids, fluid motion will have small effect on the flux to small planktonic organisms, such as bacteria, but will be important for large phytoplankton cells and osmotrophic larvae. Chains and filaments, in particular, are expected to experience enhanced relative motion if their lengths approach the Kolmogorov scale. Fluid motion can be very significant, however, to small cells that feed on large dissolved molecules or colloids as implied from the inverse dependence of *Sh* on the diffusion coefficient. The dependence of *Sh* on cell size differs among the mechanisms by which relative motion can be induced (Table 3). Hence, optimal cell size will vary with this changing dependence (Jumars et al. 1993). This result may provide one explanation for the existence of such a wide range of phytoplankton sizes. While the theory that relates cell size and mass transfer is well developed, there is clear need for more laboratory experiments. The size range that has been examined so far is very narrow and limited to small cells, mainly bacteria.

A striking feature of the phytoplankton community is its diversity of shapes and morphologies. Analytic solutions for mass transfer to shapes other than spheres are limited to spheroids and cylinders. Solutions for more complex shapes require numerical modelling. It has been suggested that spines and horns, common features in many phytoplankton species, are devices that increase drag and thereby decrease sinking speeds or are means to thwart grazers (Sournia 1982). An additional function of horns and spines may be to increase the effective size of cells without changing volume or gross catabolic rate, so that absolute length will exceed the Kolmogorov scale or at least Batchelor's (1952) diffusional length scale (Table 4). Chain formation can serve a similar purpose, especially if cells are held apart from each other so that their diffusionally depleted layers do not overlap. While cells in a chain can remain as small units, the total length of the chain may be long enough to experience the curvature of a turbulent flow and gain benefit from the relative difference in velocity. Terminal cells would experience the greatest relative motion, and chain flexibility would influence absolute amounts of motion experienced and their time variation.

Although most osmotrophs live at low Reynolds numbers with viscous forces smoothing out velocity gradients, the potential flow fields experienced by cells are varied, and comparably diverse strategies can be used by cells of various species to alter their physical environments and hence their diffusional fluxes. In such an unsteady environment as the upper mixed layer there is no one strategy that will maximize nutrient transfer to the cell at all times or for all cell sizes.

Acknowledgments

We thank K. Banse, H. Berg, T. Daniel, N. Franzen, G. Jackson, J. Lazier, B. Logan, K. Mann, A.R.M. Nowell, M.J. Perry, J. Shimeta and P. Yager for constructive comments on early versions of the manuscript. We are grateful to H. Berg for re-examining and sharing the details of his numerical model. LuAnne Thompson kindly provided her "big machine" for running our numerical model. This study was supported by ONR Grants N00014-94-1-0656 and N00014-94-0264.

References

Acrivos, A. & Goddard, J. D. 1965. Asymptotic expansions for laminar forced-convection heat and mass transfer. *Journal of Fluid Mechanics* **23**, 273–91.

Acrivos, A. & Taylor, T. D. 1962. Heat and Mass transfer from single spheres in Stokes flow. *Physics of Fluids* **5**, 387–94.

Amon, M. W. & Benner, R. 1994. Rapid cycling of high-molecular-weight dissolved organic matter in the ocean. *Nature* **369**, 549–52.

Baker M. A. & Gibson, C. H. 1987. Sampling turbulence in the stratified ocean: statistical consequences of strong intermittency. *Journal of Physical Oceanography* **17**, 1817–36.

Batchelor, G. K. 1952. Small-scale variation of convected quantities like temperature in turbulent fluid. *Journal of Fluid Mechanics* **5**, 113–33.

Batchelor, G. K. 1979. Mass transfer from a particle suspended in fluid with a steady linear ambient velocity distribution. *Journal of Fluid Mechanics* **95**, 369–400.

Batchelor, G. K. 1980. Mass transfer from small particles suspended in turbulent fluid. *Journal of Fluid Mechanics* **98**, 609–23.

Beklemishev, C. W. 1959. Sur la colonialité des diatomées planctoniques. *Internationale revue der Gesamten Hydrobiologie* **44**, 11–26.

Berdalet, E. 1992. Effects of turbulence on the marine dinoflagellate Gymnodinium nelsonii. *Journal of Phycology* **28**, 267–72.

Berg, H. C. & Purcell, E. M. 1977. Physics of chemoreception. *Biophysical Journal* **20**, 193–219.

Berg, H. C. & Turner, L. 1995. Cells of Escherichia coli swim either end forward. *Proceedings of the National Academy of Sciences of the United States of America* **92**, 477–9.

Bowen, J. D., Stolzenbach, K. D. & Chisholm, S. W. 1993. Simulating bacterial clustering around phytoplankton cells in turbulent water. *Limnology and Oceanography* **38**, 36–51.

Brainerd, K. E. & Gregg, M. C. 1993. Diurnal restratification and turbulence in the oceanic surface mixed layer. 1. Observations. *Journal of Geophysical Research* **98**, 22645–22,656.

Brennen, C. & Winet, H. 1977. Fluid mechanics of propulsion by cilia and flagella. *Annual Review of Fluid Mechanics* **9**, 339–98.

Brenner, H. 1963. Forced convection heat and mass transfer at small Peclet numbers from a particle of arbitrary shape. *Chemical Engineering Science* **18**, 109–22.

Brumley, B. H. & Jirka, G. H. 1987. Near-surface turbulence in a grid-stirred tank. *Journal of Fluid Mechanics* **183**, 235–63.

Canelli, E. & Fuhs, G. W. 1976. Effect of the sinking rate of two diatoms (Thalassiosira spp.) on uptake from low concentrations of phosphate. *Journal of Phycology* **12**, 93–9.

Chwang, A. T. & Wu, T. Y. 1971. A note on the helical movement of micro-organisms. *Proceedings of the Royal Society of London, Series B, Biological Sciences* **178**, 327–46.

Clift, R., Grace, J. R. & Weber, M. E. 1978. *Bubbles, drops and particles*. New York: Academic Press.

Confer, D. R. & Logan, E. L. 1991. Increased bacterial uptake of macromolecular substrates with fluid shear. *Applied and Environmental Microbiology* **57**, 3093–100.

Crank, J. 1975. *The Mathematics of Diffusion*, 2nd edn. Oxford: Clarendon Press.

Culver, M. E. & Smith, W. O. 1989. Effects of environmental variation on sinking rates of marine phytoplankton. *Journal of Phycology* **25**, 262–70.

Cussler, E. L. 1984. *Diffusion, mass transfer in fluid systems*. Cambridge: Cambridge University Press.

Dorrepaal, J. M. & O'Neill, M. E. 1979. The existence of free eddies in a streaming Stokes flow. *Quarterly Journal of Mechanics and Applied Mathematics* **32**, 95–107.

Dortch, Q., Thompson, P. A. & Harrison, P. J. 1991. Variability in nitrate uptake kinetics in *Thalassiosira pseudonana* (Bacillariophyceae). *Journal of Phycology* **27**, 35–9.

Eppley, R. W., Holmes, R. W. & Strickland, D. H. 1967. Sinking rates of marine phytoplankton measures with a fluorometer. *Journal of Experimental Marine Biology and Ecology* **1**, 191–208.

Fenchel, T. 1987. *Ecology of protozoa*. Berlin: Springer.

Forgacs, O. L. & Mason, S. G. 1959. Particle motions in sheared suspensions X. Orbits of flexible threadlike particles. *Journal of Colloid Science* **14**, 473–91.

Frankel, A. N. & Acrivos, A. 1968. Heat and mass transfer from small spheres and cylinders freely suspended in shear flow. *Physics of Fluids* **11**, 1913–18.

Friedlander, S. K. 1957. Mass and heat transfer to single spheres and cylinders at low Reynolds numbers. *American Institute of Chemical Engineering Journal* **3**, 43–8.

Gargett, A. E. 1989. Ocean turbulence. *Annual Review of Fluid Mechanics* **21**, 419–51.

Gavis, J. 1976. Munk and Riley revisited: nutrient diffusion transport and rates of phytoplankton growth. *Journal of Marine Research* **34**, 161–79.

Goldman, J. C. 1984. Conceptual role for microaggregates in pelagic waters. *Bulletin of Marine Science* **35**, 462–76.

Goldsmith, H. L. & Mason, S. G. 1961. Axial migration of particles in Poiseuille flow. *Nature* **190**, 1095–6.

Goldsmith, H. L. & Mason, S. G. 1967. The microrheology of dispersion. In *Rheology*, F. R. Eirich (ed.). New York: Academic Press, 85–250.

Happel, J. & Brenner, H. 1965. *Low Reynolds number hydrodynamics*. New Jersey: Prentice-Hall.

Hutchinson, G. E. 1967. *A treatise on limnology. Vol. II: Introduction to lake biology and the limnoplankton*. New York: John Wiley.

Jackson, G. A. & Lochmann, S. 1993. Modeling coagulation of algae in marine systems. In *Environmental particles*, J. Buffle & H. P. van Leeuwen (eds). Lewis Publishers, 387–414.

Jeffery, D.J. & Sherwood, J. D. 1980. Streamline patterns and eddies in low-Reynolds-number flow. *Journal of Fluid Mechanics* **96**, 315–34.

Jumars, P. A. 1993. *Concepts in biological oceanography*. New York: Oxford University Press.

Jumars, P. A., Deming, J. W., Hill, P. S., Karp-Boss, L., Yager, P. L. & Dade, W. B. 1993. Physical constraints on marine osmotrophy in an optimal foraging context. *Marine Microbial Food Webs* **7**, 121–59.

Kamykowski, D. & McCollum, S. A. 1986. The temperature acclimatized swimming speed of selected marine dinoflagellates. *Journal of Plankton Research* **8**, 275–87.

Kamykowski, D., Reed, R. E. & Kirkpatrick, G. J. 1992. Comparison of sinking velocity, swimming velocity, rotation and path characteristics among six marine dinoflagellate species. *Marine Biology* **113**, 319–28.

Karnis, A., Goldsmith, H. L. & Mason, G. S. 1963. Axial migration of particles in Poiseuille flow. *Nature* **200**, 159–60.

Keller, S. R. & Wu, T. Y. 1977. A porous prolate-spheroidal model for ciliated micro-organisms. *Journal of Fluid Mechanics* **80**, 259–78.

Kiørboe, T. 1993. Turbulence, phytoplankton cell size, and the structure of pelagic food webs. *Advances in Marine Biology* **29**, 1–72.

Koch, A.L. 1971. The adaptive responses of Escherichia coli to a feast and famine existence. *Advances in Microbial Physiology* **6**, 147–217.

Korson, L., Dorst-Hansen, W. & Millero, J. F. 1969. Viscosity of water at various temperatures. *Journal of Physical Chemistry* **73**, 34–9.

Kramer, H. 1946. Heat transfer from spheres to flowing media. *Physica* **12**, 61–80.

Kronig, R. & Bruijsten, J. 1951. On the theory of the heat and mass transfer from a sphere in a flowing medium at low values of Reynolds' number. *Applied Scientific Research* **A2**, 439–46.

Kutateladze, S. S., Nakoryakov, V. E. & Iskakov, M. S. 1982. Electrochemical measurements of mass transfer between a sphere and a liquid in motion at high Péclet numbers. *Journal of Fluid Mechanics* **125**, 453–62.

Lazier, J. R. N. & Mann, K. H. 1989. Turbulence and diffusive layers around small organisms. *Deep-Sea Research* **36**, 1721–33.

Leal, G. L. 1980. Particle motions in a viscous fluid. *Annual Review of Fluid Mechanics* **12**, 435–76.

Leal, G. L. 1992. *Laminar flow and convective transport processes*. Boston: Butterworth-Heinemann.

Li, Y. H. & Gregory, S. 1974. Diffusion of ions in sea water and in deep-sea sediments. *Geochimica et Cosmochimica Acta* **38**, 703–14.

Lighthill, J. 1986. *An informal introduction to theoretical fluid mechanics*. Oxford: Clarendon Press.

Logan, E. L. & Dettmer, J. W. 1989. Increased mass transfer to microorganisms with fluid motion. *Biotechnology and Bioengineering* **35**, 1135–44

Logan, E. L. & Hunt, J. R. 1987. Advantages to microbes of growth in permeable aggregates in marine systems. *Limnology and Oceanography* **32**, 1034–48.

Logan, E. L. & Hunt, J. R. 1988. Bioflocculation as a microbial response to substrate limitations. *Biotechnology and Bioengineering* **31**, 91–101.

Logan, E. L. & Kirchman, D. L. 1991. Uptake of dissolved organics by marine bacteria as a function of fluid motion. *Marine Biology* **111**, 175–81.

Maddock, J. R. & Shapiro L. 1993. Polar location of the chemoreceptor complex in the Escherichia coli cell. *Science* **259**, 1717–23.

Malone, T. C. 1980. Algal size. In *The physiological ecology of phytoplankton*, I. Morris (ed.). California: University of California Press, 433–63.

Mann, K. H. 1992. Physical influences on biological processes: how important are they? *South African Journal of*

Marine Science **12**, 107–21.
Mann, K. H. & Lazier, J. R. N. 1991. *Dynamics of marine ecosystems*. Boston: Blackwell Scientific.
Margalef, R. 1978. Life-forms of phytoplankton as survival alternatives in an unstable environment. *Oceanologica Acta* **1**, 493–509.
Masliyah, J. H. & Epstein, N. 1972. Numerical solution of heat and mass transfer from spheroids in steady axisymmetric flow. *Progress in Heat and Mass Transfer* **6**, 613–32.
McLaughlin, J. B. 1991. Inertial migration of a small sphere in linear shear flow. *Journal of Fluid Mechanics* **224**, 261–74.
McNown, J. S. & Malaika, J. 1950. Effects of particle shape on settling velocity at low Reynolds numbers. *Transactions, American Geophysical Union* **31**, 74–82.
Mierle, G. 1985. Kinetics of phosphate transport by Synechococcus leopoliensis (Cyanophyta): evidence for diffusion limitation on phosphate uptake. *Journal of Phycology* **21**, 177–81.
Mitchell, J. G. 1991. The influence of cell size on marine bacterial motility and energetics. *Microbial Ecology* **22**, 227–38.
Monin, A.S. & Yaglom, A. M. 1975. *Statistical fluid mechanics: mechanics of turbulence. Vol 1*. Cambridge: The MIT Press.
Morel, F. M. M., Hudson, R. J. M. & Price, N. M. 1991. Limitation of productivity by trace metals in the sea. *Limnology and Oceanography* **36**, 1742–55.
Munk, W. H. & Riley, G. A. 1952. Absorption of nutrients by aquatic plants. *Journal of Marine Research* **11**, 215–40.
Oakey, N. S. & Elliott, J. A. 1982. Dissipation within the surface mixed layer. *Journal of Physical Oceanography* **12**, 171–85.
Osborn, T. R. & Lueck, R. 1985. Turbulence measurements with a submarine. *Journal of Physical Oceanography* **15**, 1502–20.
Parkinson, J. S. & Blair, D. F. 1993. Does E. coli have a nose? *Science* **259**, 1701–2.
Pasciak, W. J. & Gavis, J. 1974. Transport limitation of nutrient uptake in phytoplankton. *Limnology and Oceanography* **19**, 881–8.
Pasciak, W. J. & Gavis, J. 1975. Transport limited nutrient uptake rates in Ditylum brightwellii. *Limnology and Oceanography* **20**, 604–17.
Press, W. H., Tevkolsky, S. A., Vetterling, W. T. & Flannery, B. P. 1992. *Numerical recipes in C*. 2nd edn. Cambridge: Cambridge University Press.
Purcell, E. M. 1977. Life at low Reynolds number. *American Journal of Physics* **45**, 3–11.
Purcell, E. M. 1978. The effect of fluid motions on the absorption of molecules by suspended particles. *Journal of Fluid Mechanics* **84**, 551–9.
Raven, J. A. 1982. The energetics of freshwater algae: energy requirements for biosynthesis and volume regulation. *New Phytologist* **92**, 1–20.
Raven, J. A. & Richardson, K. 1984. Dinophyte flagella: a cost-benefit analysis. *New Phytologist* **98**, 259–76.
Riebesell, U., Wolf-Gladrow, D. A. & Smetacek, V. 1993. Carbon dioxide limitation of marine phytoplankton growth rates. *Nature* **361**, 249–51.
Roberts, A. M. 1981. Hydrodynamics of protozoan swimming. In *Biochemistry and physiology of protozoa*, M. Levandowsky & S. H. Hunter (eds). New York: Academic Press, 5–66.
Rohsenow, W. M. & Choi, H. Y. 1961. *Heat, mass and momentum transfer*. New Jersey: Prentice-Hall.
Saffman, P. G. 1965a. The lift on a small sphere in a slow shear flow. *Journal of Fluid Mechanics* **22**, 385–400.
Saffman, P. G. 1965b. Corrigendum. *Journal of Fluid Mechanics* **31**, 624 only.
Savidge, G. 1981. Studies of the effects of small-scale turbulence on phytoplankton. *Journal of the Marine Biology Association of the United Kingdom* **61**, 477–88.
Sergé, G. & Silberberg, A. 1961. Radial particle displacement in Poiseuille flow of suspensions. *Nature* **189**, 209–10.
Shay, T. S. & Gregg, M. C. 1986. Convectively driven turbulent mixing in the upper ocean. *Journal of Physical Oceanography* **16**, 1777–98.
Shimeta, J. 1993. *Mechanisms and rates of particle encounter among suspension feeders*. PhD thesis, University of Washington, USA.
Shimeta, J., Jumars, P. A. & Lessard, E. J. 1995. Influences of turbulence on suspension feeding by planktonic protozoa: experiments in laminar shear fields. *Limnology and Oceanography* **40**, 845–59.
Smayda, T. J. 1970. The suspension and sinking of phytoplankton in the sea. *Oceanography and Marine Biology: an Annual Review* **8**, 353–414.
Smetacek, V. S. 1985. Role of sinking in diatom life-history cycles: ecological, evolutionary and geological signifi-

cance. *Marine Biology* **84**, 239–51.
Sommer, U. 1988. Some size relationships in phytoflagellate motility. *Hydrobiologia* **161**, 125–31.
Sournia, A. 1982. Form and function in marine phytoplankton. *Biological Reviews of the Cambridge Philosophical Society* **57**, 347–94.
Spiegel, M. R. 1959. *Vector analysis*. New York: McGraw-Hill.
Taylor, G. I. 1935. Statistical theory of turbulence. *Proceedings of the Royal Society of London, Series A*, **151**, 421–44.
Tennekes, H. & Lumley, J. L. 1972. *A first course in turbulence*. Cambridge: The MIT Press.
Thomas, W. H. & Gibson, C. H. 1990a. Quantified small-scale turbulence inhibits a red tide dinoflagellate, Gonyaulax polyedra Stein. *Deep-Sea Research* **37**, 1583–93.
Thomas, W. H. & Gibson, C. H. 1990b. Effects of small-scale turbulence on microalgae. *Journal of Applied Phycology* **2**, 71–7.
Thomas, W. H. & Gibson, C. H. 1992. Effects of quantified small-scale turbulence on the dinoflagellate, Gymnodinium sanguineum (splendens): contrast with Gonyaulax (Lingulodinium) polyedra, and the fishery implication. *Deep-Sea Research* **39**, 1429–37.
Throndsen, J. 1973. Motility in some marine nannoplankton flagellates. *Norwegian Journal of Zoology* **21**, 193–200.
Titman, D. & Kilham, P. 1976. Sinking in freshwater phytoplankton: some ecological implications of cell nutrient status and physical mixing processes. *Limnology and Oceanography* **21**, 409–17.
Van de Ven, T. G. M. & Mason, S. G. 1976. The microrheology of colloidal dispersions. VI. Chains of spheres in shear flow. *Journal of Colloid and Interface Science* **57**, 535–46.
Van Duuren, F. 1968. Defined velocity gradient model flocculator. *Journal of the Sanitary Engineering Division Proceedings of the American Society of Civil Engineers SA* **4**, 671–82.
Van Ierland, E. T. & Peperzak, L. 1984. Separation of marine seston and density determination of marine diatoms by density gradient centrifugation. *Journal of Plankton Research* **6**, 29–44.
Waite, A. M., Thompson, P. A. & Harrison, P. J. 1992. Does energy control the sinking rates of marine diatoms? *Limnology and Oceanography* **37**, 468–77.
Yamazaki, H. & Lueck, R. 1990. Why oceanic dissipating rates are not lognormal. *Journal of Physical Oceanography* **20**, 1907–18.

Appendix I Notation

Symbol	Definition	Dimensions
A	cell surface	L^2
C	concentration of a given nutrient	mol L^{-3}
C_∞	ambient concentration, far from the cell surface	mol L^{-3}
C_0	concentration at the cell surface	mol L^{-3}
C^*	dimensionless concentration (C/C_∞)	dimensionless
D	diffusion coefficient	L^2T^{-1}
$\mathbf{E}$	rate of strain tensor	T^{-1}
E	shear rate $E \equiv \lvert\mathbf{E}\rvert$	T^{-1}
E_{ij}	the ij component of the strain rate tensor $E_{ij} = \frac{1}{2}\left(\frac{\partial U_i}{\partial X_j} + \frac{\partial U_j}{\partial X_i}\right)$	T^{-1}
$\bar{E}$	mean shear rate	T^{-1}
E_ω	component of the strain rate tensor parallel to the direction of rotation	T^{-1}
e	perturbation strain rate	T^{-1}
e_{ij}	the ij component of the perturbation strain rate tensor $e_{ij} = \frac{1}{2}\left(\frac{\partial u_i'}{\partial X_j} + \frac{\partial u_j'}{\partial X_i}\right)$	T^{-1}

Symbol	Definition	Dimensions
f	nondimentional drag on the cell	dimensionless
$\mathbf{G}$	velocity gradient tensor	T^{-1}
G_{ij}	the ij component of the velocity gradient tensor	T^{-1}
g	gravitational acceleration	LT^{-2}
k	mass transfer coefficient	LT^{-1}
K_m	concentration at which uptake equals $1/2V_{max}$	$molL^{-3}$
L_c	characteristic length scale	L
$\boldsymbol{n}$	unit vector inward normal to the body surface	dimensionless
P	ratio between diffusion and maximal uptake rates (Pasciak & Gavis 1974)	dimensionless
Pe	Péclet number, $Pe \equiv \frac{UL_c}{D}$	dimensionless
Pe_{shear}	Péclet number in shear flow, $Pe \equiv \frac{EL_c^2}{D}$	dimensionless
$Pe_{turbulence}$	Péclet number in turbulence, $Pe \equiv \frac{r_0^2}{D}\left(\frac{\varepsilon}{\nu}\right)^{\frac{1}{2}}$	dimensionless
Q	total flux arriving to the cell in the presence of fluid motion	mol $cell^{-1}$ T^{-1}
Q_D	purely diffusional flux	mol $cell^{-1}$ T^{-1}
r	radial distance from the centre of the cell	L
r_0	cell radius	L
r^*	nondimensional radial distance from the centre of the cell	dimensionless
Re	Reynolds number. The ratio between inertial and viscous forces, $Re \equiv \frac{UL_c}{\nu}$	dimensionless
Re_s	Reynolds number of a cell based on its swimming velocity, $Re \equiv \frac{U_{swimming}L_c}{\nu}$	dimensionless
Re_{shear}	Reynolds number of a cell based on the shear flow, $Re \equiv \frac{EL_c^2}{\nu}$	dimensionless
Sh	Sherwood number, $Sh \equiv \frac{Q}{Q_D} \equiv \frac{kr_0}{D}$	dimensionless
Sh_0	Sherwood number in the case of pure diffusion	dimensionless
t_D	characteristic time scale for diffusion	T
U	characteristic velocity ($U = U_1, U_2, U_3$)	LT^{-1}
$\mathbf{U}$	velocity field	LT^{-1}
U^*	dimensionless velocity field ($\mathbf{U}/U$)	dimensionless
$\bar{U}$	mean velocity	LT^{-1}
U_∞	far-field velocity	LT^{-1}
$U_{sinking}$	sinking velocity	LT^{-1}
$U_{swimming}$	swimming velocity	LT^{-1}
U_s	swimming or sinking velocity	LT^{-1}
U_s^*	Component of swimming or sinking velocity parallel to the axis of rotation	LT^{-1}
U_{shear}	characteristic velocity of the shear flow	LT^{-1}
$U_{transverse}$	velocity of passive migration	LT^{-1}
$U_{turbulence}$	characteristic velocity of sub-Kolmogorov turbulent flow	LT^{-1}
u'	perturbation velocity	LT^{-1}
$\mathbf{V}$	mean free velocity of the shear flow	LT^{-1}
V_{max}	maximal uptake rate	mol $cell^{-1}$ T^{-1}
$\boldsymbol{X}$	position vector $X = (x_1, x_2, x_3) = (x, y, z)$	-
ε	kinetic energy dissipation rate of the flow	L^2T^{-3}
η	Kolmogorov length scale (of the smallest eddies associated with the shear flow)	L
η_b	Batchelor length scale (of the smallest fluctuations in the concentration field)	L

Symbol	Definition	Dimensions
γ	shear rate for simple shear flow	T^{-1}
∇	del operator that indicates partial derivatives in three spatial dimensions; in Cartesian co-ordinates, $\frac{\partial}{\partial x}+\frac{\partial}{\partial y}+\frac{\partial}{\partial z}$	L^{-1}
∇^*	dimensionless del operator	dimensionless
μ	dynamic viscosity	$ML^{-1}T^{-1}$
ν	kinematic viscosity	L^2T^{-1}
Ω	rotation rate tensor	T^{-1}
Ω_{ij}	the ij component of the rotation rate tensor, $\Omega_{ij}=\frac{1}{2}\left(\frac{\partial U_i}{\partial X_j}-\frac{\partial U_j}{\partial X_i}\right)$	T^{-1}
ρ	density of the medium in which cells are immersed	ML^{-3}
ρ_c	mean density of the cell	ML^{-3}
ϑ	Kolmogorov scale of velocity	LT^{-1}

Appendix 2 Advection–diffusion model

We solved numerically for concentration distributions of nutrients around a spherical cell at low Reynolds number under unidirectional flow and linear shear ($Re \ll 1$). The concentration field around the cell for both flow regimes is given by Equation 7 with the boundary conditions 8 and 9, where, for spherical co-ordinates,

$$\nabla^2 C=\frac{1}{r^2}\frac{\partial}{\partial r}\left(r^2\frac{\partial C}{\partial r}\right)+\frac{1}{r^2\sin\theta}\frac{\partial}{\partial\theta}\left(\sin\theta\frac{\partial C}{\partial\theta}\right)+\frac{1}{r^2\sin^2\theta}\frac{\partial^2 C}{\partial\phi^2}$$

and

$$\nabla C=\hat{r}\frac{\partial C}{\partial r}+\frac{\hat{\theta}}{r}\frac{\partial C}{\partial\theta}+\frac{\hat{\phi}}{r\sin\theta}\frac{\partial C}{\partial\phi}.$$

The velocity field **U** depends on the flow regime. For unidirectional, uniform flow past a sphere, **U** is composed of two components, U_r and U_θ, where (Leal 1992)

$$U_r=\left(1-\frac{3}{2r}+\frac{1}{2r^3}\right)\cos\theta \text{ and } U_\theta=\left(1-\frac{3}{4r}-\frac{1}{4r^3}\right)\sin\theta .$$

Since the problem is axisymmetric, velocity and concentration do not depend on the second angular co-ordinate, ϕ ($\partial/\partial\phi = 0$). The velocity field of the shear flow (uniaxial extensional flow where $\mathbf{E} = (2,0,0;\ 0,-1,\ 0;\ 0,0,-1)$ also comprises two components, U_r and U_0, where (Leal 1992)

$$U_r=\left(r-\frac{5}{2r^2}+\frac{3}{2r^4}\right)\left(3\cos^2\theta-1\right) \text{ and } U_0=-3\left(r-\frac{1}{r^4}\right)\sin\theta\cos\theta .$$

For each flow field, we nondimensionalized by cell radius, free velocity (far from the cell) and concentration at the domain boundary. Due to symmetry, only one-half the domain was

computed, with an additional no-flux boundary condition at the angular boundary ($\partial C/\partial\theta = 0$ at $\theta = 0, \pi$). In order to increase resolution near the cell the radial independent variable r was replaced by the variable $\mu = \ln(r)$. The grid (μ-θ co-ordinates) was composed of 231 points with constant radial separation ($\Delta\mu$) and 101 points with constant angular separation ($\Delta\theta$). Computation of the concentration at each point was marched in time using upwind difference. The first-order spatial derivative was calculated from central differencing and the second-order spatial derivative was calculated using ADI (alternating direction implicit) following Press et al. (1992, Ch. 19). The model was run until satisfactory steady state was reached, i.e. when the change in *Sh* was smaller than 10^{-4} for one nondimensional time step (r_0^2/D). Boundary conditions 9 cannot be applied as given in the text since $r = \infty$ is not part of the domain. Therefore we used $C(r_{max}) = 1-(1/r_{max})$, the value obtained from the analytic solution for pure diffusion. The solution for the problem with this boundary condition will converge to the exact solution as grid size increases toward infinity. For small *Pe* we chose the domain boundary to be $O(100r_0)$ and tested model sensitivity to it by doubling domain size. For large *Pe* values the domain we needed was of $O(1000r_0)$ since the effect of the cell on the concentration field extends to a larger distance. Berg & Purcell (1977) used a similar model but with a smaller domain (H. Berg, pers. comm.). Our sensitivity analysis with our own model suggests that their domain might not extend far enough to include the flow variation contained in Stokes' solution. We believe that this truncation of the flow and concentration field is the principal reason for the discrepancy between their model and the asymptotic analytic solutions and our numerical model.